View metadata, citation and similar papers at core.ac.uk
brought to you by CORE
provided by IntechOpen

We are IntechOpen, the world's leading publisher of Open Access books Built by scientists, for scientists

4,800
Open access books available

122,000
International authors and editors

135M
Downloads

154
Countries delivered to

Our authors are among the
TOP 1%
most cited scientists

12.2%
Contributors from top 500 universities

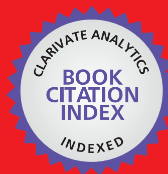

WEB OF SCIENCE™

Selection of our books indexed in the Book Citation Index in Web of Science™ Core Collection (BKCI)

Interested in publishing with us? Contact book.department@intechopen.com

Numbers displayed above are based on latest data collected.
For more information visit www.intechopen.com

10

Monte-Carlo Simulation in Electron Microscopy and Spectroscopy

Vladimír Starý
Czech Technical University in Prague, Czech Republic

1. Introduction

In electron microscopy, spectroscopy and microanalysis, knowledge of certain quantities is very often needed for proper analytical measurement. Unfortunately, the real values of some of these quantities can only be roughly estimated for two reasons: the complicated process of electron and phonon transport through the matter can be only very approximately described by the analytical theory, and the experimental measurement of some quantities for proper evaluation of experiments is hardly possible. In this case, a Monte-Carlo simulation (MC) can give us reasonable results (see reviews (Berger, 1963), (Binder, 1979), (Joy, 1995), (Dapor, 2003)). As the main motivations of Monte-Carlo simulations in electron microscopy and spectroscopy we can put

a. calculation of inelastic mean free path (IMFP) of electrons in matter,
b. prognostics of the physical processes results.

The reliability of Monte-Carlo models is usually checked by comparison with experimental results; unfortunately, some quantities can be measured only indirectly or with some experimental problems. The basic problems lie

a. in selecting suitable quantities, which can be at best directly measured and the results of calculations can be compared with them;
b. in maximizing the range of these quantities for which the checking is valid (electron energy, atomic number, thickness of surface film, etc.)

When this method was first used, due to the low speed of computers, the multiple scattering type of calculation was usually used, and the relatively long parts of the path were simulated simultaneously using averaging of scattering effects. Nowadays, so-called single scattering models are employed, where each scattering event is calculated individually. In Monte-Carlo code, both the formulas and tables of values necessary for calculation can be used. Because of necessity of interpolation of values between values given by tables, the formulas are preferred.

In the energy range used for electron microscopy, spectroscopy and microanalysis (i.e., usually 0.1 to 300 keV), various models are used in MC codes for describing the basic interactions of electrons with atoms - elastic and inelastic collisions and other interactions of electrons with materials.

2. Description of the physical interactions of electrons with material

Interaction of particle A_1 with nucleus A_2 is described generally by formula

$$A_1 + A_2 \Rightarrow A_3 + A_4 + Q, \tag{1}$$

where A_3 is the outgoing particle, A_4 is resulting nucleus and Q is emitted energy.

2.1 Elastic scattering

For elastic scattering, the simulation started using the Rutherford formula (usually with unscreened or screened nucleus charge and sometimes with relativistic correction). Now more exact calculation of differential cross sections is provided by using the static field approximation of atomic potential (Dirac-Hartree-Fock-Slater, Thomas-Fermi-Dirac, etc.) with relativistic partial wave analysis (e.g., (Salvat & Mayol, 1993), (Mayol & Salvat, 1997), (Salvat et al., 2005)). Moreover, the Hartree-Fock-Wigner-Seitz (muffin-tin) potential can be used for atoms in the solid state. In recent years, several comprehensive codes calculating the differential cross-sections (DCS) and total cross-sections (TCS) have been published for energies down to very low values (Bote et al., 2009); the database of the total and transport cross-sections is also available (Jablonski et al., 2003).

The appearance of energy losses due to bremsstrahlung radiation is an important process in "elastic" electron scattering by matter. The process of generating continuum radiation, i.e., an energy loss in "elastic" collisions, is due to the change of electron direction connected with photon emission and some additional deceleration. The differential cross-section of photon production with frequency ω, after a change in electron direction from $\mathbf{v}_0$ to $\mathbf{v}$ (a change in electron direction given by angle γ) and with angle θ between the direction of the incoming electron and photon emission, has been calculated theoretically by several authors (Landau & Lifshic, 1974), (Kirkpatrick & Wiedmann, 1945), (Chapman et al., 1983), (Kissel et al., 1983). Because the cross-sections of bremsstrahlung excitation are relatively very low comparing with other precesses, this process is usually omitted.

According to the laws of energy and momentum conservation this means that at electron-nucleus collision some energy is transferred to the nucleus and is thus lost by electron. Due to the big difference between masses of electron and nucleus, the energy transfer to nucleus is usually, e.g., at energies used in electron microscopy and microanalysis, very low, in order of meV. Only at relatively high electron energy (e.g., at TEM) and low atomic number samples (biological samples, polymers etc.) the electron energy loss can be remarkable. According the formula in (Reimer, 1984), the loss at collision of 100 keV electron with carbon nucleus depends on electron scattering angle, at 0.5 and 180 degree being 4.3 meV and 226 eV, respectively.

2.2 Inelastic scattering

For simple solution, the simple model of continuous slowing down (CSD) can be employed. In the more exact single scattering calculations, we need to know the inelastic cross sections. The calculation of inelastic differential cross-sections is usually slightly more complicated due to the complicated interaction of charged particle with matter having the various dielectric structure. Moreover, the inelastic cross-section is double differentiated - by change of momentum (depending on scattering angle) and by electron energy loss. For MC simulations we need to calculate the inelastic mean free path (IMFP) and the stopping power for given electron energy and element/material; at inelastic event the result should give us the energy loss and scattering angle.

According to the Bethe theory, the electrons in matter are represented by the system of oscillators and electrons lose energy due to their excitation. If we suppose discrete spectrum M of oscilators with energy states W_i and the responsible oscilator strengths f_i, then we have for stopping power S

$$S = -\frac{dE}{dz} = \frac{\pi e^4}{(4\pi\varepsilon_0)^2}\frac{N_1}{E}\sum_{i=1}^{M} f_i \ln\left(\frac{E}{W_i}\right)^2 = \sigma_0 \frac{N_A}{EA}\sum_{i=1}^{M} Z_{nl}\ln\left(\frac{E}{E_{nl}}\right)^2 . \quad (2)$$

$\sigma_0 = \pi e^4/(4\pi\varepsilon_0)^2 = 6.51\ 10^{-20}$ keV^{2}cm^2, N_1 being the number of atoms in a volume unit ($N_1 = N_A\rho/A$, ρ the density in g/cm^3, or $N_1 = N_A/A$ if we use mass thickness in μg/cm^2), N_A Avogadro number, A the atomic mass, E electron energy in keV and z the path length in μg/cm^2. In original Bethe solution, due to the condition $\sum_{i=1}^{M} f_i = Z$, in the some approximation we can similarly estimate f_i by electron number at given atomic (sub)shell Z_i and W_i by the energy of electrons at these shells by E_{nl}. This was realized in (Reimer & Stelter, 1986); because of some atomic electrons, especially the outer ones, can result in too large energy losses, the corrected values of Z_i and W_i were used. By definition of the mean ionisation potential J (in eV units) according the condition $\sum_{i=1}^{M} f_i \ln W_i = Z \ln J$ we obtain from (2) the simple formula for so called continuous slowing down approximation of electrons in material

$$S_B = 2\pi e^4 \frac{N_1 Z}{E}\ln\left(\frac{1.166E}{J}\right), \quad (3a)$$

Z being the atomic number and J the mean ionisation potential, which can depend on Z. The empirical formula for J used in the most works on electron probe microanalysis (EPMA), according to (Berger & Seltzer, 1964), is as follows

$$J/Z = 0.015 \text{ for } Z \le 13 \quad (4a)$$

and

$$J/Z = 9.76 + 58.5^{-0.19} \text{ for } Z > 13. \quad (4b)$$

In practice we can use for the Bethe stopping power formula

$$S_B = 7.85\times 10^3 \frac{Z\rho}{AE}\ln\left(\frac{1.166E}{J}\right) \text{ [eV/nm]}. \quad (3b)$$

The stopping power S characterizes the energy loss per unit path length (negative derivation of energy dependence on the path length). In reality, the energy losses are not continuous and the “struggling”, the large energy losses, may appear as drops in this dependence. The approximation also causes the divergency of S at decreasing of electron energy to zero. Moreover, the S, which should increase with decreasing energy, starts to decrease at about $E = 6.338\ J$. Thus for lower energies the formula for S can be corrected by empirical corrections - either by the Rao-Sahib & Wittry (RSW) correction (Rao-Sahib & Wittry, 1974) or by the Joy & Luo (JL) correction (Joy & Luo, 1989), also widely used in EPMA calculations. RSW correction is used for energies E < 6.338 J, then we have for S_B the formula (the coefficient ensures the continuity of S_B at the energy E = 6.338 J)

$$S_B = 6.236 \times 10^3 \frac{Z\rho}{A\sqrt{EJ}} \ \text{[eV/nm]}. \tag{5}$$

In the JL correction, instead of mean ionisation potential J the corrected value J' is used in equation (3),

$$J' = \frac{J}{1 + kJ / E}, \tag{6}$$

where k = 0.77 - 0.85 for various elements.
Differential cross-section (DCS) of inelastic collision in Born approximation is (Inokuti, 1971)

$$\frac{d^2\sigma}{dWdQ} = \frac{\pi e^4}{E} \frac{1}{WQ} \frac{df(W,Q)}{dW}, \tag{7}$$

where E is energy of primary electron, W energy loss, Q energy given by momentum change ($Q = \hbar^2 q^2 / 2m$), $\hbar$ **q** momentum change, **q**=**k**-$\mathbf{k_0}$, $\mathbf{k_0}$ and **k** are wave vectors of impinging and outgoing electrons, $\mathbf{k_0}$= $2\pi\lambda_e$, λ_e is the electron wavelength and $df(Q,W)/dW$ is the generalised oscillator strength (GOS) density, which gives the interaction magnitude between electron and target. Integrating the inelastic DCS over all scattering angles, the inelastic scattering is described by energy loss distribution (loss function) $f(W)$ which can be approximated by relatively simple formula. In (Liljequist, 1978) the function $f(W)$ is defined as

$$f(W) = \frac{d\sigma_{in}(W)}{dW} \bigg/ \int_{W_{\min}}^{W_{\max}} \frac{d\sigma_{in}(W)}{dW} dW, \tag{8}$$

where $d\sigma_{in}(W)/dW$ is the differential inelastic cross section, integrated over the whole solid angle. Then, on the base of supposition of binary collisions of followed electron with electrons of material it was assumed that generally the dependence of $f(W)$ on energy loss W is as follows

$$f(W) = HW^{-2} \tag{9}$$

in the interval (W_{min}, W_{max}) and $f(W)$=0 in ($0, W_{min}$), $W_{min} > 0$. W_{max} and W_{min} are the limits of electron energy loss in matter. We can use simply W_{max} = E, the actual energy of an electron, W_{min} is a constant, which does not change during the electron path. H is the constant which can be calculated by normalization of $f(W)$. If we assume the distribution (9) (hyperbolic), the normalization of $f(W)$ to unity, i.e.

$$\int_{W_{\min}}^{E} f(W')d'W = 1 \tag{10}$$

gives

$$H = \frac{EW_{\min}}{E - W_{\min}}. \tag{11}$$

In (Liljequist, 1978)), the same shape of $f(W)$ and the same value of W_{min} (10 eV) for all the elements was assumed, but better, W_{min} may be taken as an adjustable parameter. By this way

$$f(W) = \frac{EW_{\min}}{E - W_{\min}} W^{-2} \cong W_{\min} W^{-2} , \tag{12}$$

($E >> W_{min}$), and we can calculate the actual energy loss W at each inelastic event by a way similar to that usually used in the Monte-Carlo codes, by means of the random number R $(0 \le R \le 1)$ and the formula

$$\int_{W_{\min}}^{W} f(W')dW' = R. \tag{13}$$

Due to our knowledge of $f(W)$, we can also simply calculate W_m, the mean energy loss,

$$W_m = \int_{W_{\min}}^{E} W\, f(W)dW \cong W_{\min} \ln\left(\frac{E}{W_{\min}}\right), \tag{14}$$

knowing W_m the IMFP (in equations denoted as Λ_{in}) can be calculated as

$$\Lambda_{in} = \frac{W_m}{S_B} . \tag{15}$$

The advantage of this definition is the presence of only one parameter W_{min} for optimizing the agreement of the Monte-Carlo and experimental values, for example the coefficient of elastic reflection R_e. So, the energy dependence of IMFP is defined by (15) after including (3) and (14), taking into account corrections of S_B for low energy region. Even though it is not exact shape of loss function $f(W)$, the simplicity for fitting of some experimental data is advantageous.

The other possibility is to utilize the supposed analytical shape of energy distribution of losses at inelastic scattering. In the Tougaard theory (Tougaard, 1997), the basic formula for $f(E,W)$ is

$$f(W) = \frac{BW}{\left(C + W^2\right)^2} \tag{16}$$

which is used usually for materials with broad band of energy losses, e.g., Au and Cu (Tougaard, 1997). Here W is the energy loss and B and C are the constants. According to normalisation

$$\int_0^\infty f(E,W)dW = \frac{B}{2C} = 1 . \tag{17}$$

we have $B=2C$. In this formulas, $f(W)$ does not depend on the primary energy of electron E. Then from (16) and (17) we can directly write

$$W_m = \int_0^\infty W f(E,W)dW = \int_0^\infty \frac{BW^2}{\left(C + W^2\right)^2} dW = \frac{\pi B}{4\sqrt{C}} . \tag{18}$$

The suggested modification (Starý et al., 2007) can be accomplished by implementation of the energy dependence of the loss function into the Tougaard's formula (16). We carried it out as follows: first, normalisation of the distribution was performed within the limits (0,*E*) (*E* being the actual energy of electron) instead of (0,∞), which made the former constant B in equation (19) energy-dependent as follows

$$B = \frac{2C(C+E^2)}{E^2}. \tag{19}$$

Putting equations (18) into (15), and integrate in the limits (0,*E*), the integral can be solved analytically

$$W_m = \int_0^E W f(E,W)dW = \frac{C(C+E^2)}{E^2}\left(\frac{1}{\sqrt{C}}arctg\frac{E}{\sqrt{C}} - \frac{E}{C+E^2}\right). \tag{20}$$

After calculation of W_m, we can obtain the proper values of constants C and using (19) also B in the analytical shape of energy distribution (16). Then, using the Bethe stopping power S_B corrected for low energies according to (Joy & Luo, 1989), we calculated the possible values of IMFP with C as a free parameter for various energies between 0.1 and 20.0 keV. These values were compared with the valid values of IMFP obtained from TPP-2 formula (Tanuma et al., 1991a). The best fit gives the energy dependent value of C in Tougaard's formula (16) and modified Tougaard's Universal cross section *f(E,W)* can be found. The equation (20) can be also solved directly to find the energy dependence of C using a suitable iteration code. By this way, we obtained for C the approximate formula $C = -0.0155{*}E^2+0.529{*}E+1.8785$ and $C = -0.0173{*}E^2 +0.6402{*}E+2.1312$ (C[keV^2], E[keV]), in the case of Cu and Au, respectively. Then the energy loss can be calculated according to (13).

At given energy loss, the scattering angle is derived using several suppositions (Raether, 1980):

a. scattering angle ϑ_c is in interval <0, ϑ_{max});
b. there is obeyed rule $\vartheta_{\max} = \sqrt{2\vartheta_p} = \sqrt{W_p / E}$, energy W_{max} is given by $W_{\max} = \sqrt{4W_pE}$;
c. if $W < W_p$, then scattering angle is $\vartheta_c = 0$;
d. if $W_p < W < W_{max}$, then scattering angle is $\vartheta_c = \sqrt{\left(W - W_p\right) / 2\alpha_R E}$, α_R is a constant defined in (Raether, 1980);
e. if $W > W_{max}$, the binary collision (electron-electron scattering) takes place and scattering angle is given by formula $\sin^2 \vartheta_c = W / E$.

W_p is energy of bulk plasmon (for carbon W_p = 25.9 eV, for copper and gold there is a relatively complicated structure of energy losses); in our code we suppose W_p = 30 eV and 20 eV, respectively;

Except these relatively simple conditions of inelastic scattering the more exact theories appeared. According (Fernandez-Varea et al., 1996) "the calculation of inelastic DCS starts either from the Bethe theory for the inelastic scattering of fast electrons from free atoms or from the dielectric theory for the energy loss of charged particles in condensed matter".

Differential cross-section (DCS) of inelastic collision in Born approximation is given in Bethe theory by (7). Using the GOS density *df(Q,W)/dW,* the quantum mechanical Bethe sum rule (instead summing we use now integration)

$$\int_0^\infty \frac{df(Q,W)}{dW} dW = Z \tag{21}$$

is obeyed for any Q. In the limit $Q \to 0$ the GOS becomes equal to the optical oscillator strength (OOS) density $df(0,W)/dW \equiv df(W)/dW$ which describes the excitation of free atom by photons in the dipole approximation.
For binary collisions the scattering angle ϑ is given by formula (Liljequist, 1983)

$$Q = 2E - W - 2\sqrt{E(E-W)}\cos\theta \tag{22}$$

The inelastic mean free path Λ and stopping power $S = -dE/ds$ are then given as (Liljequist, 1983)

$$\frac{1}{\Lambda} = N_1 \int_Q d\sigma \, , \tag{23}$$

$$S = N_1 \int_\Omega W d\sigma \, , \tag{23}$$

the mass thickness is used in IMFP and S, and integration proceeds over space given by kinematic conditions $\Omega'(W,\Omega)$. The exact solution of this theory now enables to calculate DCS, IMFP and stopping power for energies of electrons and positrons between 10 eV and 1GeV (Bote et al., 2009), (Fernandez-Varea et al., 2005). In (Fernandez-Varea et al., 1993), it is possible to find the suitable approximative formulas for calculation of both of IMFP and S.
Some theories use dielectric theory and optical data and calculate the inelastic mean free path and the stopping power by different way, e.g., (Pines, 1964), (Tung et al., 1979), (Ritchie, 1982), (Penn, 1987), (Ding & Shimizu, 1989). The inverse inelastic mean free path is given as

$$\frac{d^2\Lambda^{-1}}{d\omega dq} = \frac{me^2}{\pi\hbar E}\frac{1}{q}\mathrm{Im}\left(\frac{-1}{\varepsilon(q,\omega)}\right) \tag{24a}$$

where q is momentum change of electron and ω is a frekvency giving the energy transfer from electron at inelastic collision , $W = \hbar\omega$. Because $\Lambda = 1/(N_1\sigma)$ and $Q = \hbar^2 q^2 / 2m$, we also have

$$\frac{d^2\sigma}{dWdQ} = \frac{me^2}{2\pi\hbar^2}\frac{1}{N_1 E}\frac{1}{Q}\mathrm{Im}\left(\frac{-1}{\varepsilon(q,\omega)}\right). \tag{24b}$$

The dielectric response of material with more or less free electron gas and by this way also the IMFP is intensively studied. For free-electron-like material, as e.g. Al and Si, the calculation of $\mathrm{Im}(-1/\varepsilon(\omega))$ agree very well with the experimental excitation spectrum and contain sharp peak at plasmon energy and several edges due to deep inner shels. Also the theoretical plasmon dispersion relation agrees with experiments, mainly for low q's (Raether, 1980). For transition metals and noble metals, the improved method was suggested by (Penn, 1987) and then used in (Tanuma et al., 1987, 1991a, 1991b, 1993, 1994) for calculation of IMFP not only for elements, but also of compounds including organic

compounds. It employs directly the experimental data of $\varepsilon(\omega)$ for expansion of Im(-1/$\varepsilon(\omega,q)$) into infinite series of Drude-Lindhard terms, thus avoiding any fitting parameters. The question of stopping power was solved in (Ding & Shimizu, 1989), where the energy dependences for Al, Si, Ni, Cu, Ag and Au are calculated. The results are different from the Bethe theory for electron energy < 10 keV, for energies 0.1 - 3 keV the differences are substantial.

For practical use, in (Tanuma et al., 1991a) the relatively simple expressions, denoted as TPP-2, are deduced, where the values of IMFP are obtained using material constans for electron energy 0.1 to 2 keV. They are as follows

$$\Lambda_{in} = \frac{E}{E_p^2\left[\beta \ln(\gamma E)\right] - \frac{C}{E} + \frac{D}{E^2}}, \ [10^{-1}\text{nm}] \tag{25}$$

where β = -0.0216 + 0.944/(E_p^2 + E_g^2)$^{1/2}$ + 7.39·10$^{-4}\rho$, γ = 0.191$\rho^{1/2}$, C = 1.97-0.91U, D = 53.4+20.8U a $U = N_v\rho/M$, ρ is the density [g/cm^3], E_p = 28.8U$^{1/2}$ is plasmon energy and E_g is the energy gap width for semiconductors (in eV), N_v number of valence electrons and M atomic or molecular mass. This formula which is usually denoted as TPP-2 gives the possibility to define IMFP of elements, semiconductors and organic materials; sometimes the more exact formula TPP-2M (Tanuma et al., 1993) is utilized.

2.3 Surface energy losses

In recent years, the energy losses of an electron transmitted through the surface have been intensively studied. These losses are connected with surface plasmon excitations. The mean number of excited surface plasmons P_s, which is denoted also as SEP, the surface excitation parameter, can be theoretically given as a function of the electron energy E and the surface transmission angle ϑ, i.e., the angle between the trajectory of the electron and the direction perpendicular to the surface. There are several suggested formulas for SEP, namely (Chen, 1996)

$$P_s = \frac{a}{\sqrt{E}\cos\vartheta}, \tag{26}$$

where a is the fitting parameter, mentioned in (Chen, 1996) for several materials. Formerly, also another formula

$$P_s = \frac{b}{\sqrt{E}\cos\vartheta}\left[\left(\frac{\pi}{2} - \vartheta\right)\cos\vartheta + \sin\vartheta\right] \tag{27}$$

was published by the same authors (Chen, 1995). Then, in (Oswald, 1992) forP_s the other formula was suggested

$$P_S(\vartheta, E) = \frac{1}{a\sqrt{E}\cos\vartheta + 1}, \tag{28}$$

where a is a parameter which, for nearly free electron gas materials, is given as a_{NFE} = $(8a_o/\pi^2e^2)^{1/2}$ (Werner et al., 2001b). The coefficients a/a_{NFE} for elements with other electronic structure can be estimated from the predictive formula in (Werner et al., 2001b).

Usually, a Poisson distribution is assumed for the number of excited surface plasmons. Thus, the probability to excite n plasmons is

$$P_n = \frac{P_s^{\,n}}{n!}\exp(-P_s)\,, \tag{29}$$

and the probability to not excite any plasmon, i.e., to be transmitted without an energy loss, is simply

$$P_0 = \exp(-P_s). \tag{30}$$

Transmission of electrons both into and out of the sample should be taken into account. In the MC code, at each surface transmission the energy and the transmission angle are known. Thus, firstly the SEP is calculated and the random number R is generated. Then, the normalised accumulated probabilities F_n of excitations of 0, 1,..., i,... plasmons were calculated as $F_n = \sum_{i=0}^{n} P_i$, where P_i is the probability of generating i plasmons given by (29), until its value exceeds the generated random number, i.e., $F_n < R < F_{n+1}$. n defines the number of excited plasmons and after the electron run in the case, denoted as SEL (see below), their energy is subtracted from the energy of the electron. The abbreviations NEL and SEL will be explained in the next paragraph.

2.4 Computational details and precision estimation

There are several MC codes used frequently for calculation of electron-matter interaction, only some of them are mentioned (Gauvin & l'Esperance, 1992), (Baró et al,, 1995). Our MC calculations were realized by our code written in PASCAL language. The conditions of the calculations were set to be identical with the experimental conditions, first of all the solid angle of the detector. Usually, electrons hit to the surface perpendicularly, and the number of electrons reflected or elastically reflected or transmitted into a defined solid angle (defined by detector) were observed. In the case of elastic reflection, the electrons were divided into two groups: NEL and SEL type. Firstly, for elastic reflection, we calculated the electrons which were involved in only elastic collisions, with No Energy Loss during the path in the bulk, and in this case the energy losses at the surface excitations were omitted. The number of electrons was denoted as NEL. The number of electrons which were involved in only elastic collisions and, moreover, without Surface Energy Loss was denoted as SEL; only the electrons without any energy loss including the surface plasmon excitation are taken into account. At general reflection, the energy loss at surface is not subtracted from electron energy for NEL number, and it is subtracted for SEL number.
The hard limits of calculation were set usually to 10^6 impinging electrons, which means that the calculation was carried out for approximately 10000 - 100000 (elastically) reflected electrons into a large detector solid angle (RFA) or about 1000 - 10000 into a direction sensitive detector. In spite of low energy correction of S_B at low energies under 1 keV, its real dependence around 0.1 keV is not well defined. Moreover, when we started our simulations, the lowest energy for which the differential cross-sections of elastic scattering seem to be reasonable was about 0.1 keV for the usually used models (Salvat & Mayol, 1993) (Starý, 1999), (Starý et al., 2004). It can be supposed the decreasing of cut-off electron energy

toward 10 eV should increase calculation time very much. Thus, in our code the electrons which energy decreased under 0.1 keV is taken as absorbed. For these reasons, the minimal energy of the calculations was 0.2 keV for all elements studied. The other details do not differ from those usually used in MC codes. In all the calculations the trajectory of the electron was followed up to the escape from the sample, up the decay of electron energy under 0.1 keV or in the case of following only elastic reflection, up to the first inelastic scattering event, when the single electron run stopped. Then the data for the escaping electron was saved and a new electron started.

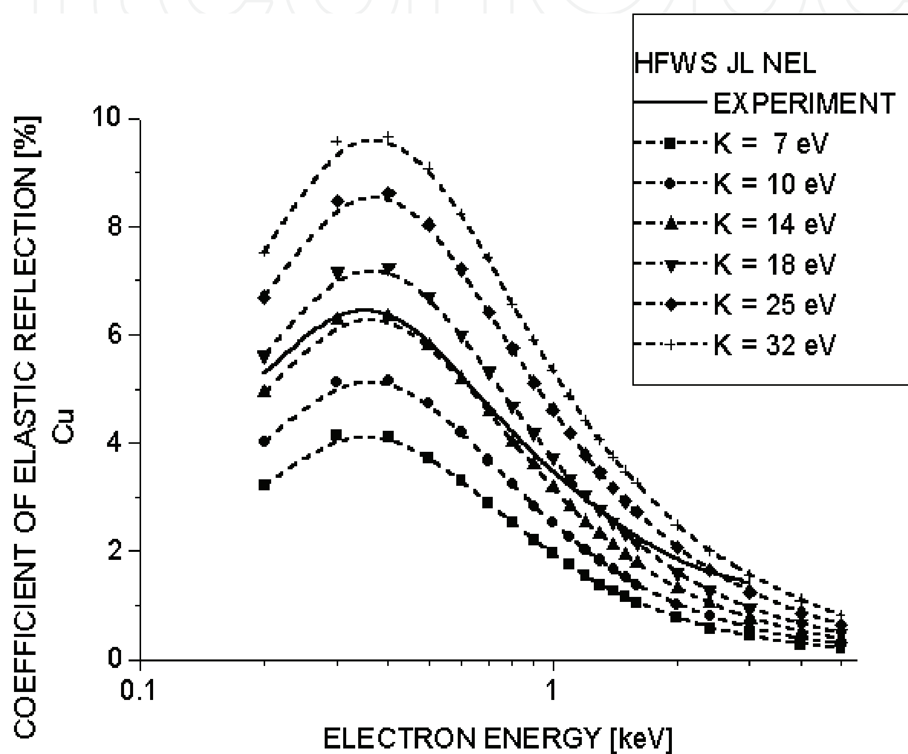

Fig. 1. Definition of optimal value of fitting parameter K for Cu. Comparison with experiment (Schmid et al., 1983).

The reliability of results, e.g., of the IMFP values, is limited by statistical errors. In the case of electron reflection from the bulk material, the number of electrons scattered to the direction sensitive detector is usually between 1500 and 8300 for Al and Au and energies 0.2 and 1.0 keV. The error of the calculated values of the number of elastically reflected electrons (and simultaneously the error of the number of electrons which have lost some energy and/or are scattered into some solid angle, i.e. the number N of electrons with a given property) can be estimated, if we assume a binomial distribution of the resulting numbers of electrons. In this case, the standard deviation can be estimated as $s = \sqrt{N_0 \hat{p}(1-\hat{p})}$, where N_0 is the full number of electrons and $\hat{p}$ is the estimated probability of this phenomenon, $\hat{p}$ =N/N_0. The upper limit of this estimation is $s_{\max} = \sqrt{N_0 / 4}$. At high number N_0 and at low value of probability $\hat{p}$ this distribution can be approximated by Poisson's distribution, and the standard deviation is approximately $\sqrt{N}$. Thus, we can estimate the relative standard deviation of calculations to be between 1% and 3%.

3. Monte-Carlo calculations and comparison with experiments

We compared our calculation with experimental values, obtained from literarature and/or obtained by cooperation with several experimental laboratories. Electron spectrometers were used for measurements of backscattered intensities. Measurements can also be made using an electron microscope of either transmission or scanning type. The reflection coefficient, the elastic reflection coefficient, the transmission of electrons through a thin foil, the chromatic error and the resolution limit due to energy losses of transmitted electrons and the size of interaction volume in bulk samples and also in thin films have been examined in a big number of experiment, which will be mentioned. The comparison and agreement between measured and calculated values was seeking mainly for the measurable quantities. In the most cases the very good agreement has been obtained.

3.1 Electron backscattering

In our works (Starý, 1999) and (Starý et al., 2004) we simulated the backscattering coefficient η and the coefficient of elastic reflection R_e of some materials. Firstly, using our MC code, we calculated elastic reflection of electrons. In these calculations the electron path was stopped after inelastic collision and this electron was not taken into the result.

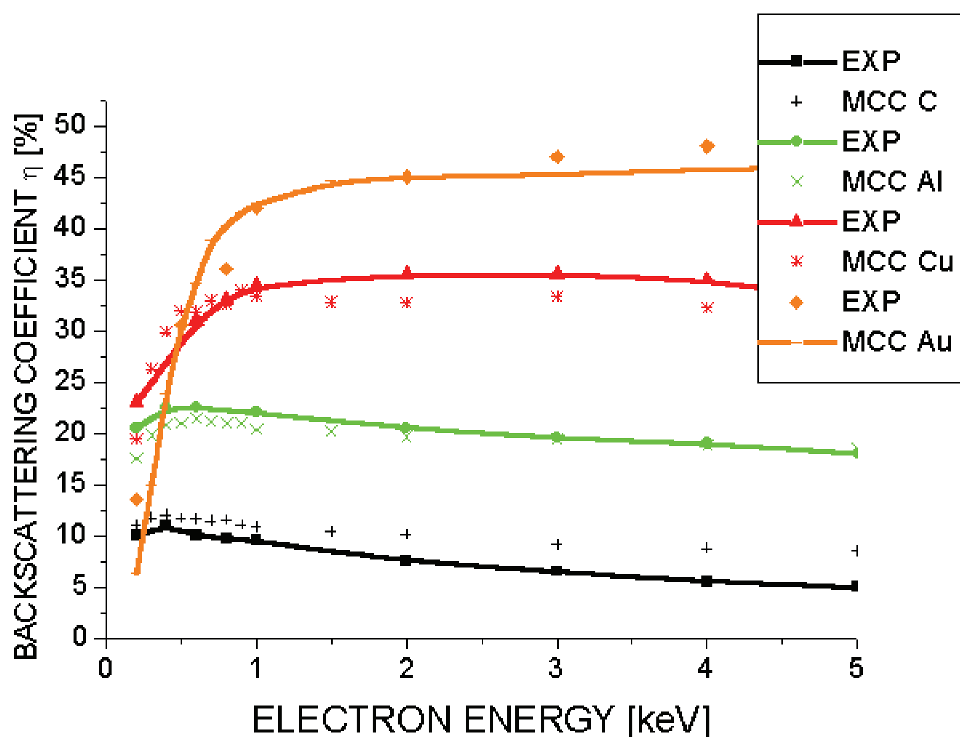

Fig. 2. The comparison of MC calculated energy dependence of backscattering coeffecient η for C, Al, Cu and Au with experiment (Fitting, 1974) (lines - measured values, points MC values).

By this way, the energy of followed electrons was the same during the whole path and instead W_{min}, only parameter K was utilized as the fitting parameter of IMFP. By integration and by comparison with experiment (e.g., with the measurement of elastic reflection) we have found the optimal value of parameter K. The example of this calculation for Cu is in

Figure 1. Optimal value of K was obtained by interpolation of values of numerical integrals of MC calculated dependences $R_e(E)$ for various K and numerical integral of experimental curve between 0.2 and 3 keV (Schmid et al., 1983). In this case, we obtained K = 17.17 eV. Using this empirical parameter given by the best agreement with measurement and equation (3), (14) - where W_{min} is replaced by K - and (15), we are able to find the energy dependence of IMFP. For practical use, e.g., for calculation of energy dependence of coefficient of backscattering η, it is possible to use these values as W_{min} in the model similar to (Liljequist, 1978) and calculate the bacscattering coefficient. Even though this model is theoretically far from reality, the energy dependence of calculated and measured values of backscattering coefficient η (Fitting, 1974) (Figure 2) shows relatively good agreement. By this way it is possible to use for simulation IMFP values from various sources and compare them. The results of simulation are shown for elastic reflection in the next paragraph.

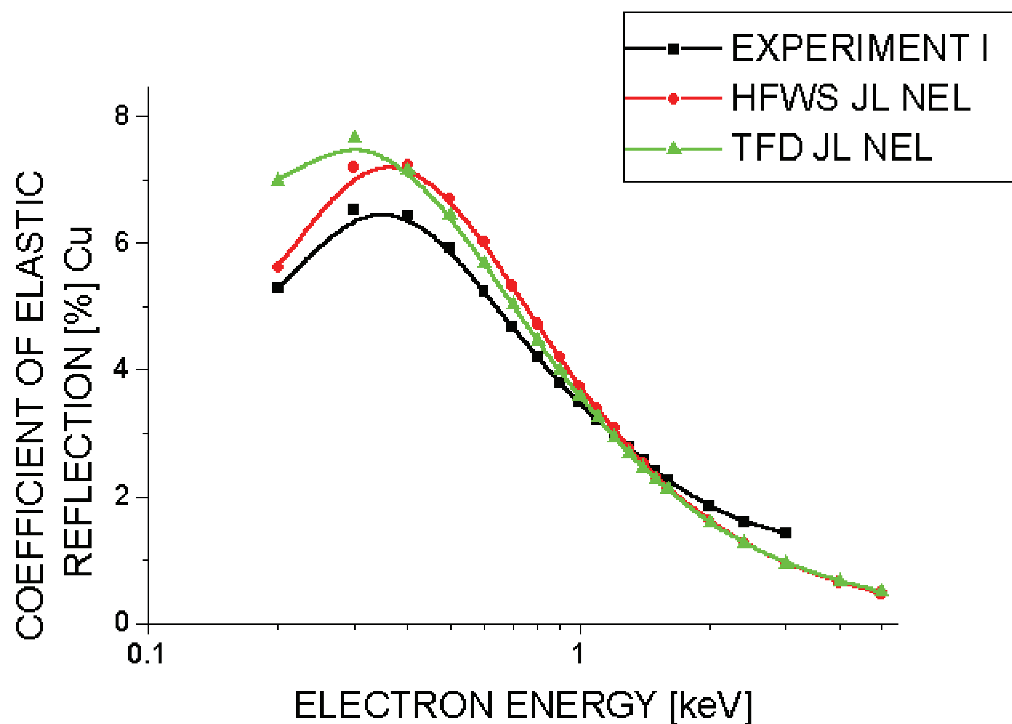

Fig. 3. The comparison of MC calculated energy dependence of coeffecient of electron elastic reflection for Cu for two models of elastic DCS with experiment (Schmid et al., 1983).

3.2 The influence of elastic and inelastic models on MC results

The next step was comparison of electron elastic reflection from several pure materials using the various physical models of elastic DCS and low energy approximation of the Bethe stopping power, and combinantions of these models, to finding the best assesments of simulated and experimental results. The results are shown in Figures 3 and 4. In Figure 3, the values of DCS are calculated by PWADIR code (Salvat & Mayol, 1993) using a static field approximation with relativistic partial wave analysis of the Dirac–Hartree–Fock and Thomas–Fermi–Dirac potential of atoms (DHF and TFD, respectively). Instead of DHF, for atoms in solid state the modified model of atomic potential (muffin-tin) denoted as HFWS model was used. Moreover, two models for improwement of low energy values of Bethe's

stopping power denoted as Joy-Luo (JL) and Rao-Sahib-Wittry (RSW) were compared (Figure 4). To define the agreement of various models of MC simulations and of the experimental curves, an evaluation of the agreement was carried out by calculating the relative differences per one measurement and calculating the residuals (Draper & Smith, 1966) and their root mean squares (RMS) – the differences between measured and calculated values of R_e in the selected range of energies between 0.2 and 3 keV. The relative differences per one set of measurement were calculated as

$$RD = \frac{100}{n}\sum_{j=1}^{n}\frac{R_{e,j}^{MC} - R_{e,j}^{\exp}}{R_{e,j}^{\exp}} \ [\%], \tag{31}$$

and the root mean squares of residuals were calculated as

$$RMS = \left(\frac{1}{n}\sum_{j=1}^{n}\left(R_{e,j}^{\exp} - R_{e,j}^{MC}\right)^2\right)^{1/2}, \tag{32}$$

n being the number of calculated values of energy (18 values). The results are given in Table 1.

	ELEMENT	C		Al		Cu		Ag		Au	
ELASTIC MODEL	S_B CORRECTION	RD [%]	RMS	RD [%]	RMS	RD [%]	RMS	RD [%]	RMS	RD [%]	RMS
HFWS	JL NEL	6.3	0.017	-5.3	0.316	1.8	0.460	41.6	2.018	12.6	0.607
	JL SEL	19.6	0.111	4.5	0.057	1.7	0.306	32.1	1.695	6.3	0.332
	RSW NEL	1.2	**0.013**	-5.1	0.293	2.9	0.476	33.0	1.787	4.4	0.390
	RSW SEL	14.0	0.104	4.0	0.062	2.4	0.492	24.6	1.500	-0.8	0.224
TFD	JL NEL	7.5	0.037	-6.6	0.377	0.8	0.574	38.1	1.855	19.5	0.672
	JL SEL	24.0	0.121	2.6	0.056	0.6	**0.170**	29.4	1.565	11.3	0.390
	RSW NEL	3.9	0.028	-6.2	0.355	1.6	0.393	29.8	1.638	8.4	0.319
	RSW SEL	17.4	0.113	1.5	**0.048**	1.5	0.251	17.2	**1.334**	1.9	**0.160**

Table 1. The agreement of measured (Schmid et al., 1983) and calculated values of R_e for several materials. The combination for each element with best fit is denoted by bold characters.

The set of energies used for RMS calculations prefers the low energy values 0.2 - 1.6 with step 0.1 keV; the next values of energy, which were 2, 2.4 and 3 keV, respectively, have less influence on the RMS value. The obtained values of RD and RMS also indicate that the results for TFD model of elastic scattering are slightly better than those for HFWS model (Table 1 and Figure 3). A comparison of the RSW and JL corrections of the stopping power (Figure 4) shows that the agreement of the calculated and experimental values of $R_e(E)$ varies for different elements. For C and Al, there is little difference between the RSW and JL corrections, for Cu the JL correction provided better agreement, for Ag and Au better agreement was provided by the RSW correction, though the RMS for Ag is large in comparison with the RMS of the best fit for the other elements. For R_e values for C, the agreement was approximately the same for JL and RSW corrections, but it was best for the NEL case (this was an exception) and HFWS model.

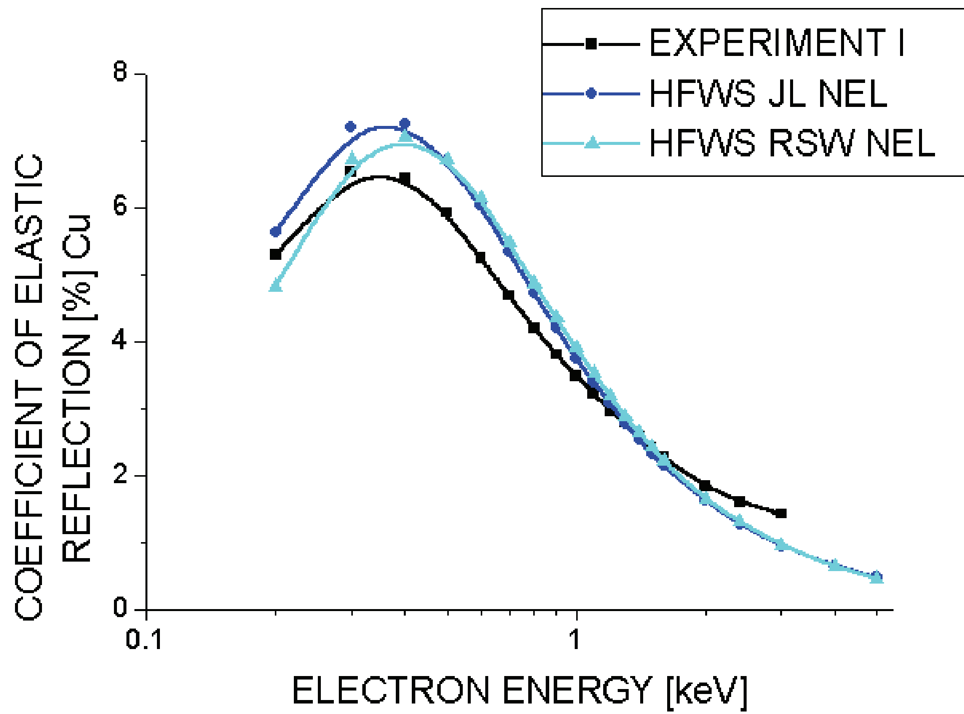

Fig. 4. The comparison of MC calculated energy dependence of coeffecient of electron elastic reflection for Cu for two models of Bethe's stopping power for low energies with experiment (Schmid et al., 1983).

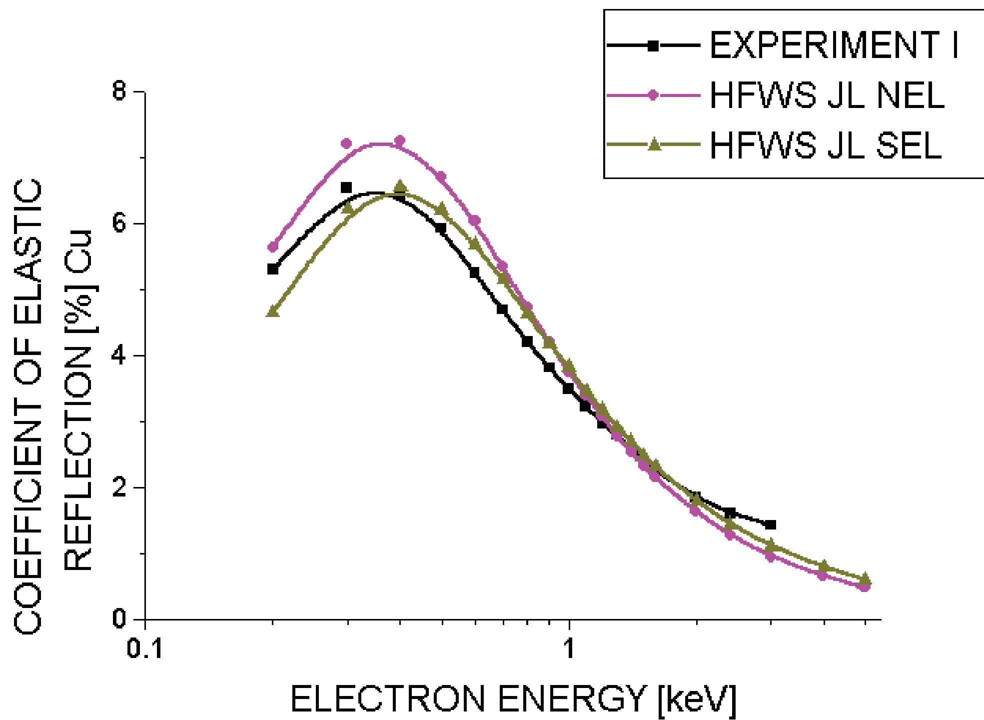

Fig. 5. The comparison of MC calculated energy dependence of coeffecient of electron elastic reflection for Cu for two models of presence of surface excitations with experiment (Schmid et al., 1983).

3.3 The influence of surface excitations

Also, using the simple model, we compared the results of experimental and MC dependence of electron elastic reflection from several materials on presence of surface excitations. We calculated the energy losses due to the surface transfer in our MC code using the surface excitation probability (SEP) P_s according to formula (28), the coefficients a/a_{NFE} for Al, Cu and Au were 0.7, 2.0 and 1.5, respectively (Werner et al., 2001b); for C and Ag the a/a_{NFE} coefficient was assumed to be 1.0 and 2.0, respectively. Transmission of electrons both into and out of the sample was taken into account. We calculated in each direction both the number of electrons reflected in this direction with No Energy Loss (NEL) in bulk and the number of electrons both without energy loss in bulk and without Surface Energy Loss (SEL).

Even a visual comparison of the results obtained without and with surface excitations into account (NEL and SEL, respectively) clearly shows that incorporating the surface excitations (SEL model) improves the agreement of the measured and calculated values of R_e for the HFWS model of elastic collisions for Al, Cu and Au (e.g., for Cu Figure 5). The preference of SEL values is clearly shown in table 1 for Al, Cu, Au and Ag.

Qualitatively, the influence of taking surface energy losses into account appears as a tilting of the MC curves around the pivot point near 1 keV. This results from the fitting method, where the area of the whole curve is fitted, but the influence of the surface excitations is more intensive for low energies.

3.4 Inelastic mean free path definition

Finding the optimal value of fitting parameter K and using value of S_B, also IMFP can be found. The MC calculated IMFP values and their dependence on energy in the observed energy range for Cu and Au are in Figures 6.a,b (TPP-2 denotes values of IMFP calculated using formula from (Tanuma et al., 1991a), FVL means values of IMFP calculated using formula in (Fernandez-Varea et al., 1993), HFWS, JL means type of elastic scattering model and low energy corrections of S_B, and NEL and SEL are the models of surface excitation. It is seen that differences between the IMFPs calculated by TPP-2 formula or formula from (Fernandez-Varea et al., 1993) are minimal. In spite of supposition, the values of IMFP found by comparison of MC and experiment using the fitting procedure are better for the NEL model then the SEL model of surface excitation. The NEL values of IMFP obtained without incorporating the surface energy losses into the calculation agree reasonably well with the theoretical values of TPP-2 (Tanuma et al., 1991a) and also those in (Fernandez-Varea et al., 1993), and for all the elements the difference lies within the range of ~10% .

The shown MC deduced IMFPs were obtained from the optimal combination of the two corrections of stopping power (RSW and JL), and for the two cases of incorporating the surface energy losses (NEL and SEL). For the resulting IMFPs the differences between the two models of elastic collisions (TFD and HFWS) are very small. For Al and Cu, the agreement of IMFP for HFWS NEL case with the theoretical values of TPP-2 is the best; for C and Cu the MC calculated values are slightly lower, and for Al, Ag and Au they are slightly higher than the theoretical values of TPP-2. The MC – NEL defined values of IMFP agree in the energy range 0.2-1.5 keV also with the IMFP values in (Ashley, 1988).

For the assessment, we used our simulated data of R_e for the set of fitting parameters to calculate IMFP from experiment (Schmid et al., 1983) for several single values of energy by the usual EPES method, employed also in (Dolinski et al, 1988a, 1988b and 1992). We

obtained the values of IMFP, very similar to those used in our MC code for generating the $R_e(E)$ with the best fit. Moreover, exchanging the experimental data of R_e for the data calculated by our code, we obtained using the EPES process exactly the IMFP used for generating R_e.

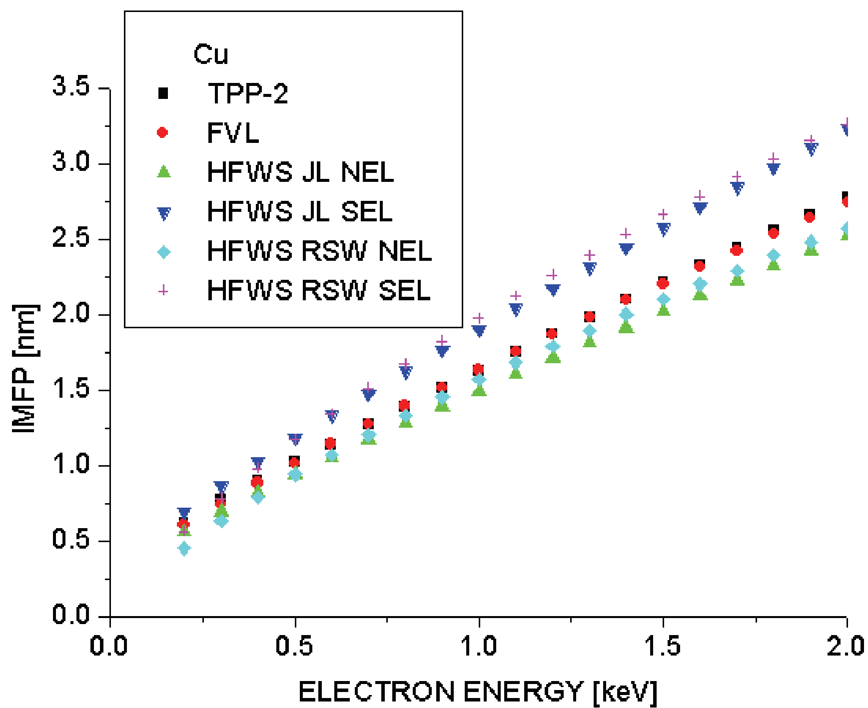

Fig. 6.a The dependence of IMFP on electron energy for Cu.

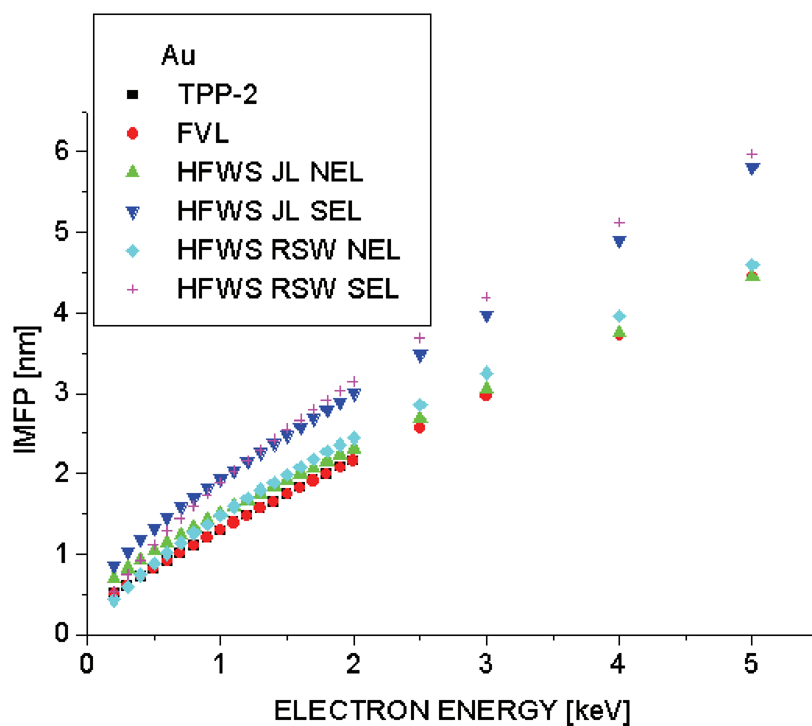

Fig. 6.b The dependence of IMFP on electron energy for Au.

When we evaluate the RFA data at single values of energy, the IMFP values deduced from MC calculations start to increase at 1.5 keV more intensively than is expected according to the TPP-2 formula. This phenomenon did not appear in our IMFP values calculated using a numerical integral. We suppose that this again results from inaccuracies of R_e measurement by RFA, which is minimised by our fitting method, inasmuch this inaccuracy has a slight influence on our IMFP values.

In evaluating the experimental data, the procedure described as „cleaning“ the experimental data from surface energy losses is sometimes used (Werner et al., 2003) and (Jung et al., 2003). Unfortunately, this procedure works only if the detector is able to resolve the angular distribution of the elastically reflected electrons. For measurements using an RFA energy analyser, where the integral values of R_e are measured, „cleaning“ cannot by carried out, because we would need to know the angular dependence of electron reflection in the experiment, i.e., the absolute $R_{e,\vartheta}$ values. In our code, „cleaning“ can be performed by fitting the R_e values by the SEL procedure, definition of optimal IMFP for it and then in NEL case of this simulation to obtain the R_e values that correspond to the „cleaned“ experimental data.

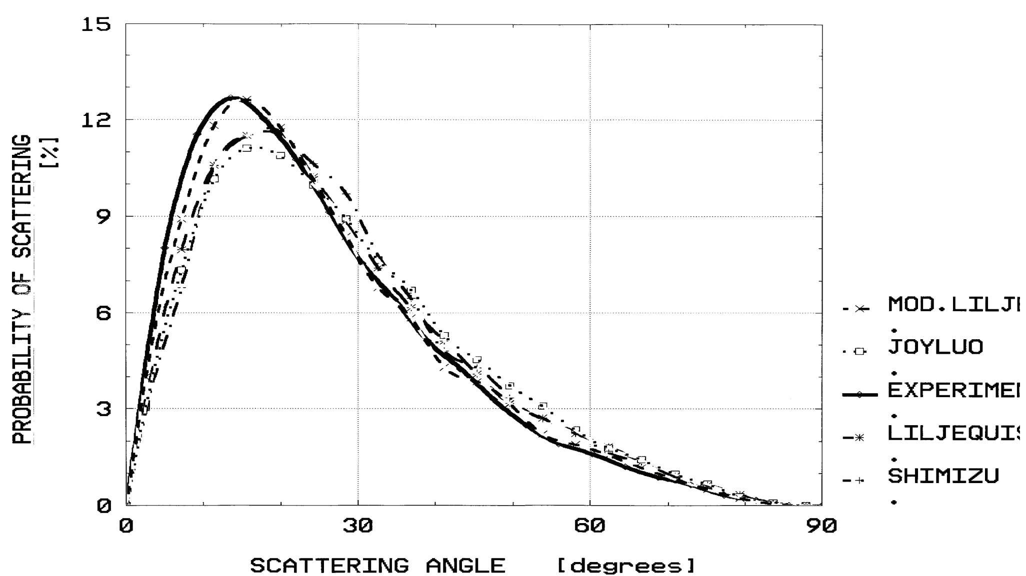

Fig. 7. Comparison of experimental and calculated values of angular distribution of transmitted electrons, and several models of inelastic scattering. Material Al, E_0 = 20 keV, film thickness 94.9 μg/cm², i.e., 351 nm. Models: MOD.LILJI≡G, JOYLUO≡D, LILJEQUI≡F, SHIMIZU≡E.

3.5 Electron transmission through the thin samples

For the oldest simulation where the DCS was given usually by analytical formulas the simplest models were used:

There was for elastic differential cross-sections

A. Rutherford's model with screened potential of nucleus (Reimer, 1984),
B. Mott's model including electron spin (according (Reimer & Lodding, 1984)),
C. tables, calculated for Hartree-Fock model of atomic potential (Riley at al., 1975),

and for inelastic differencial cross-section and IMFP

D. Bethe's continuous slowing down (CSD, at low energies using empirical correction of S_B (Joy & Luo, 1989)),
E. individual scattering using exponential distribution of energy losses (Shimizu, 1975),
F. individual scattering using hyperbolic distribution of energy losses (Liljequist, 1978),

In both E and F models the direction change comes to depend on the energy loss;

G. model, similar to F, without directional change at inelastic scattering.

We will show some comparison with experiments because also very simple models gave relatively reasonable results, even though the electron number for simulation was relatively low.

We simulated the transport of electrons of energy 10, 20, 50 and 100 keV through the thin film of C, Al, Cu and Au with thickness 20-10000 nm (Starý, 1996). The calculated data were compared with experimental values (Cosslett & Thomas, 1964a, 1964b, 1965), (Reimer et al., 1978); we evaluated

- electron backscattering coefficient,
- angular distribution of transmitted electrons,
- energy distribution of transmitted electrons.

The example of comparison of angular and energy distribution of transmitted electrons for Al and Au, respectively, and energy of primary electrons E_0 = 20 keV is in Figures 7 and 8. This comparison has two disadvantages:

- it is valid only for single material, one value of electron energy and one film thickness,
- the visual comparison is not exact.

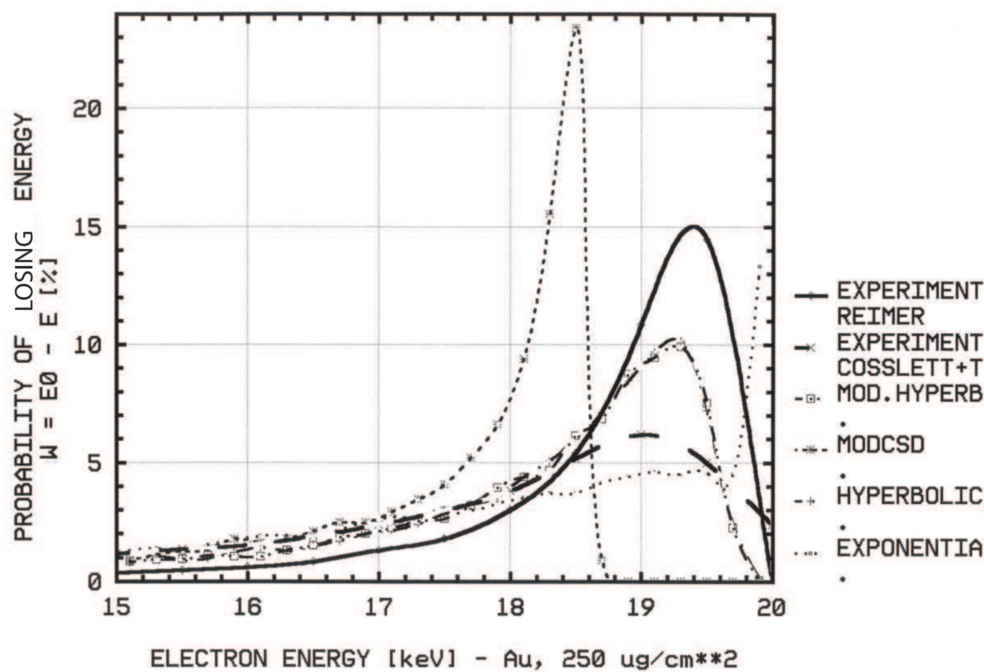

Fig. 8. The dependence of probability of energy loss W on energy of transmitted electrons for several models of inelastic scattering. Material Au, E_0 = 20 keV, film thickness 250 μg/cm^2. Models: MOD.HYPERB ≡ G, MODCSD ≡ D, HYPERBOLIC ≡ F, EXPONENTIA ≡ E.

We were therefore seeking a way to compare results simultaneously for some range of conditions (energy, thickness). Instead of coefficient of reflection η we are using the Niedrig's formula $C_N = \eta/(N_1 Z^2 d_{1/2})$, Z being the atomic number, N_1 number of atoms in

volume unit and $d_{1/2}$ the thickness of the film when the backscattering coefficient is equal to the half of the backscattering coefficient value on bulk material (Niedrig, 1982). The results of all the materials can be theoretically comprimed in one graph (excluding carbon for lack of experimental data).

For other comparison we can use residual method using squares of residuum R_s. The number of experimental results was 32 (Al, Au) and 10 (Cu). Thus we fitted 4 simulated values (for energies 10, 20, 50 and 100 keV) by function $C_N = A\,E_o^{-B}$ and experimental values were compared with C_N values calculated using fitting parameters A, B and value of energy E_i in experiments. Then

$$R_s = \frac{1}{n}\sum_{i=1}^{n}(C_{i,\exp} - AE_o^{-B}). \tag{33}$$

In the case of simulation with the same parameters (thickness, energy) as experiment, and if the number of simulations and measurements was the same, we can use other formula

$$R_s = \frac{1}{n}\sum_{i=1}^{n}(X_{i,\exp} - X_{i,calc})^2, \tag{34}$$

where $X_{i,exp}$ a $X_{i,calc}$ are the experimental and simulated values of various quantities. Lower value of R_s means better agreement with experiment. The results are in tables 2 and 3.

Model of elastic scattering	Element								
	Al			Cu			Au		
	A	B	R_s	A	B	R_s	A	B	R_s
Experiment	12913	1.922		2035	1.392		2439	1.549	
Rutherford's model	8629	1.880	839	10524	1.906	23	9513	1.847	254
Mott-Reimer's model	10598	1.947	722	6486	1.754	26	2871	1.522	30
Tables – Hartree-Fock	8860	1.816	464	6369	1.674	42	3180	1.555	12

Table 2. The comparison of experimental and calculated values of coefficients A and B (coefficients of fitting function $C_N = A\,E^{-B}$), and R_s (sum of residuum squeres) for several models of elastic scattering for Al, Cu and Au.

Model of inelastic scattering	Element		
	Al	Cu	Au
Shimizu m.	16.4	9.6	18.5
Liljequist m.	7.9	2.1	15.0
Modified Liljequist m.	4.3	1.9	5.2
CSD + Joy-Luo m.	13.3	8.9	27.3

Table 3. The R_s values from comparison of experimental and calculated values of the most probable scattering angle of transmitted electrons for Al, Cu and Au and primary energy 20 keV.

In electron microscopy and microanalysis, the MC simulation can be used to find the values of some quantities whose experimental value can be measured only with some complications. Thus, we decided to apply the MC method for low-voltage transmission

electron microscopy (LVEM). The LVEM was recently developed for observing unstained biological samples and organic thin films, and is able to work in transmission, scanning transmission and reflection modes (Delong et al., 1998). The main advantage of this method consists in the use of an accelerating voltage around 5 kV with final light microscope magnification of an electron-microscopical image. It delivers nearly twenty times more image contrast enhancement than a high voltage electron microscope using accelerating voltage 100 kV (Lednicky et al., 2000). In the case of biological specimens, staining procedures can therefore be omitted. On the other hand, such lowly-accelerated primary electrons are able to pass only through ultra thin sections, below 20 nm in thickness. Electrons accelerated by energy 5 keV are able to scatter intensively on atoms with a low atomic number including atoms of resins, which also participate in scattering and contribute to image formation. This means that the microscope is very sensitive to specimen thickness.

The aim was to show the relation between image contrast and specimen thickness, which is important for defining the sample thickness directly from electron microscopical observation, and to estimate the critical thicknesses for elastic and inelastic scattering in a sample, which characterize the possibility to observe biological samples under given conditions.

In the theory of image contrast formation in an amorphous material, an absorbtion contrast is assumed, which depends on the thickness of the sample and on its atomic number and mass (Reimer, 1984). The logarithmic contrast in electron microscopy is usually defined as $C_0 = \log N_0/N$, where N_0 and N are numbers of electrons (intensities) incident to the sample and those transferred through the objective aperture after sample transmission, respectively. The contrast of the sample can be characterized by the mass-thickness contrast parameter $S = N_A \sigma_t / A$, N_A is the Avogadro number, σ_t is the total scattering cross-section of atoms in the specimen, and A is atomic mass. Then, we can write for $C_0 = S\rho x$, ρ being the sample density, x the geometrical thickness of the specimen and $\Delta C_0 = S(\Delta\rho)x$, ΔC_0 and $\Delta\rho$ being the contrast and density differences at given thickness, respectively. Linear dependence of the contrast on the film thickness can be assumed for low density materials up to a certain critical thickness, given by the onset of multiple scattering. The characteristic “critical thickness” is defined as the thickness at which the electrons proceed on an average one elastic or inelastic scattering event during sample transmission. Next, the image is also deteriorated by inelastic scattering of the electrons, which is non-localized and decreases the image resolution.

Here, the elastic DCSs were calculated by the ELSEPA code (Salvat et al., 2005), using Dirac-Hartree-Fock with the muffin-tin atomic model. To simulate the IMFP we used values given by the TPP-2 formula (Tanuma et al., 1991a) or those obtained from our MC evaluation of absolute Elastic Peak Electron Spectroscopy.

For calculating the energy loss distribution we used the modified Tougaard’s model of the Universal cross-section of electron inelastic scattering $f(E,W)$ (Starý et al., 2007), so we were able to find the values of C for several electron energies between 0.1 and 5.0 keV. Then we found the functional dependence of C on electron energy by regression. The approximate formula is $C = 571.64 \ln(E) - 2615.9$ (C[eV^2], E[eV]). The results obtained by calculating C using TPP-2 values of IMFP were slightly different. The former method was used in our calculations. Energy loss functions calculated in this way have a reasonable shape with a maximum at about 20 - 30 eV. The amount of energy loss in an inelastic collision was obtained from the energy loss distribution by the standard Monte Carlo procedure. Then, the scattering angle was calculated either for plasmon scattering, when the scattering angle ϑ_c is between a minimum value ϑ_p (Reichelt & Engel, 1984)

$$\vartheta_p = \frac{W_p(E+E_0)}{E^2+2EE_0}, \tag{35}$$

and a maximum value ϑ_{max} = $\sqrt{2\vartheta_p}$ or by the second type of scattering, electron-electron scattering with larger energy loss (W≥ 100 eV); the scattering angles ϑ_c are also larger and they are given by the formula (Reimer, 1996)

$$\sin^2\vartheta_c = W/E \tag{36}$$

The energy of bulk plasmon is W_p=25.9 eV (Raether, 1980).
The LVEM 5 electron microscope has two objective apertures with diameter 30 and 50 μm (angular apertures 0.68 and 1.14 deg, respectively). The energy for the simulation was 5 keV, and the values of the apertures sizes for calculation were taken as 0.62 and 1.2 deg, respectively. We studied pure carbon with density between values ρ = 1.60 - 2.34 g/cm³. The hard limits of the calculation were set to 1 000 000 primary electrons.
The MC results on electron transmission show an approximately exponentially decreased number of electrons without scattering with increasing of sample thickness. The different geometrical thicknesses are given by three values of carbon density (Figure 9). Figure 10 shows the change in logarithmic contrast C for electrons with output angle $\vartheta \leq$ 11 mrad with thickness. A very low degree of nonlinearity appeared for these dependences up to 60 nm. The dependences are very similar for the two models of scattering angle distribution for inelastic scattering.

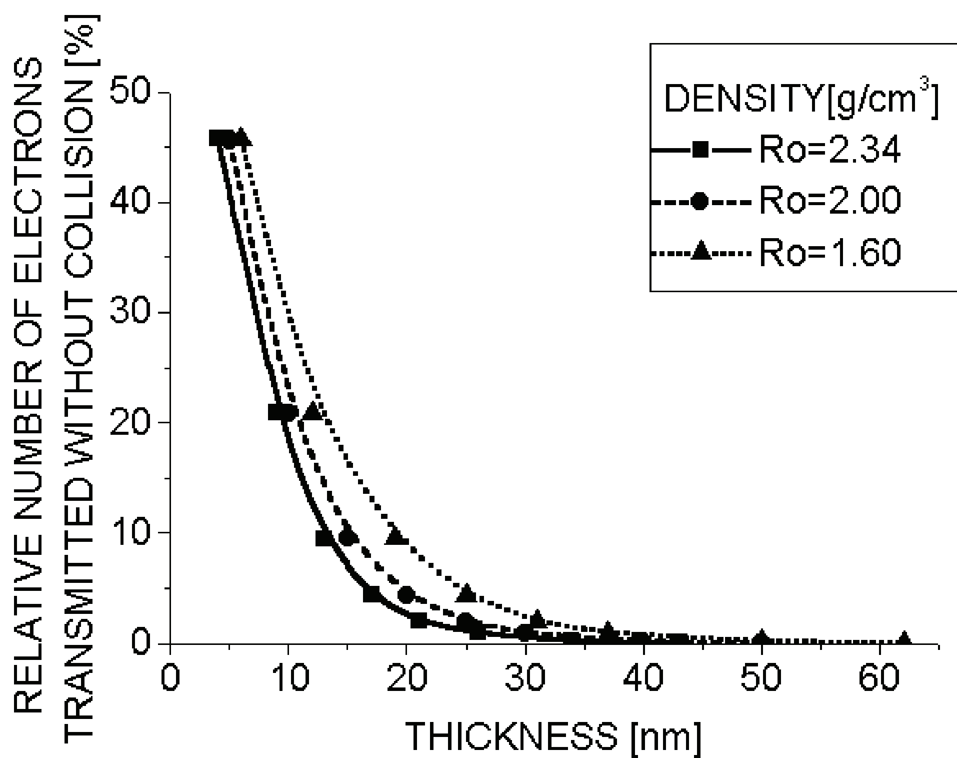

Fig. 9. Dependence of electron transmission through the film on film thickness.

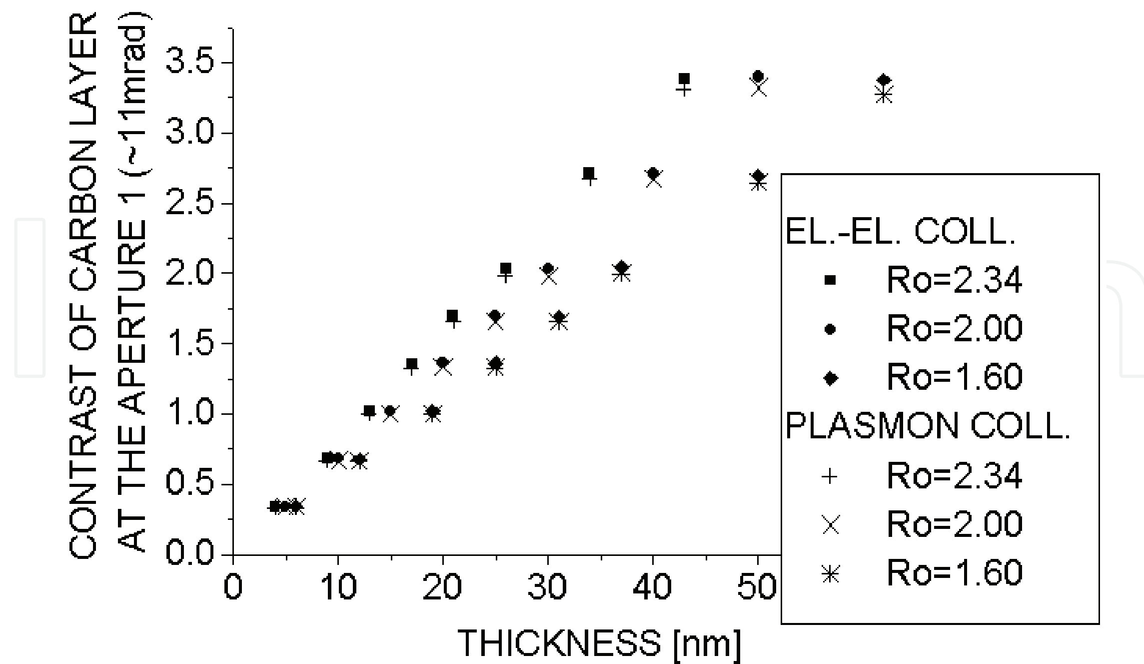

Fig. 10. Dependence of logarithmic contrast on film thickness.

DENSITY [g/cm**3]	REGRESSION EQUATION FOR ELASTIC COLLISIONS	TRANSPARENT THICKNESS [nm]		
		ELASTIC	INELASTIC	ALL
2.34	y = 0.0001x2 + 0.0614x + 0.0478	15.0	8.9	5.5
2.00	y = 0.0001x2 + 0.051x + 0.0683	17.7	10.3	6.3
1.60	y = 2E-05x2 + 0.0444x + 0.039	21.4	12.8	7.9

Table 4. Critical transparent thickness calculated for elastic, inelastic and all collisions.

The characteristic "critical thicknesses" were obtained from the dependence on thickness of the relative collision number for electrons transmitted through the film (Table 4). Because the density of a real carbon film is assumed to be higher than the density of the biological samples (about 1.6 g/cm^3), the calculated values should be the limits of microscopic observations in LVEM.
The results showing the influence of objective aperture size are shown in Figure 11. The logarithmic contrast C for all thicknesses scarcely depends on the objective aperture up to tens of miliradians, then the contrast starts to decrease. This is due to high intensity in the zero collision peak, because even at this objective aperture size the number of scattered electrons is comparable with the zero collision peak. Again, this result is the same for both models of angular distribution of inelastically scattered electrons. Finally, Figure 12 shows the dependence of the cumulative electron number (not including the zero collision peak) of electrons transmitted through the film into the aperture. Only here did a difference appear between the models of the angular distribution of inelastically scattered electrons. The calculated thickness and the angular dependences of the contrast in Figures 9 and 10 agree with the assumed values and shape of these dependencies at the energy and in the thickness range used here. The dependences in Figure 10 show the limits of the increase in contrast due to decreasing objective aperture size.

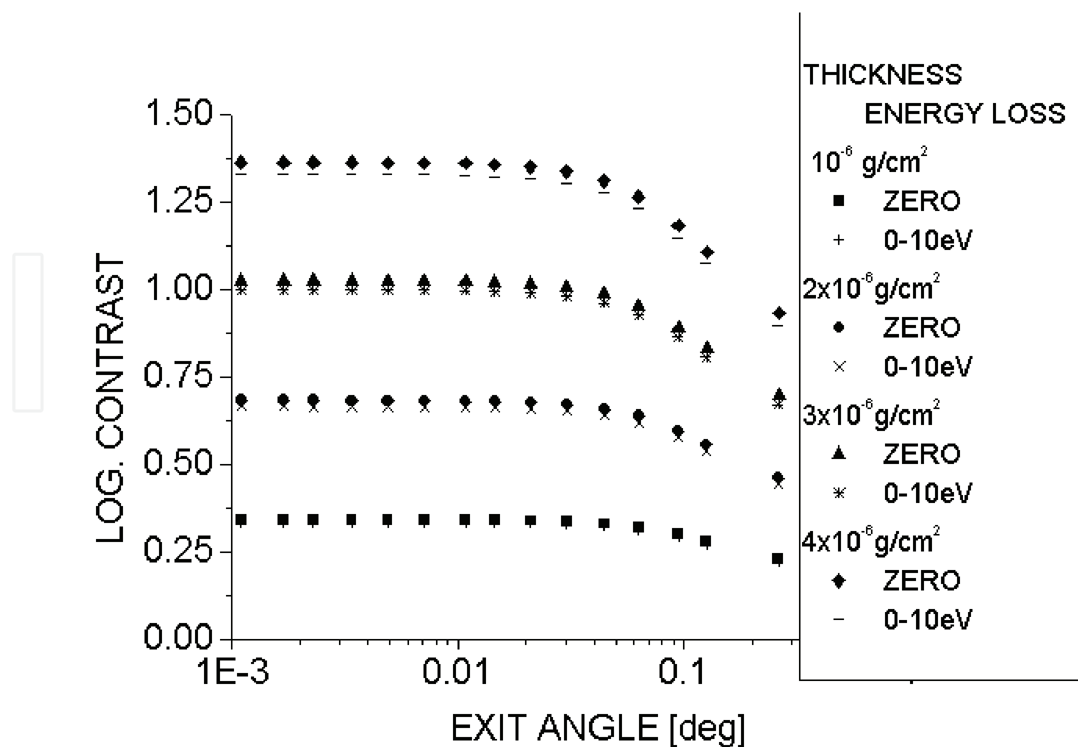

Fig. 11. Dependence of logarithmic contrast on the maximal output angle (i.e., the size of objective aperture) for electrons with ZERO energy loss and with energy loss 0-10 eV, at several values of film thickness (in g/cm^2).

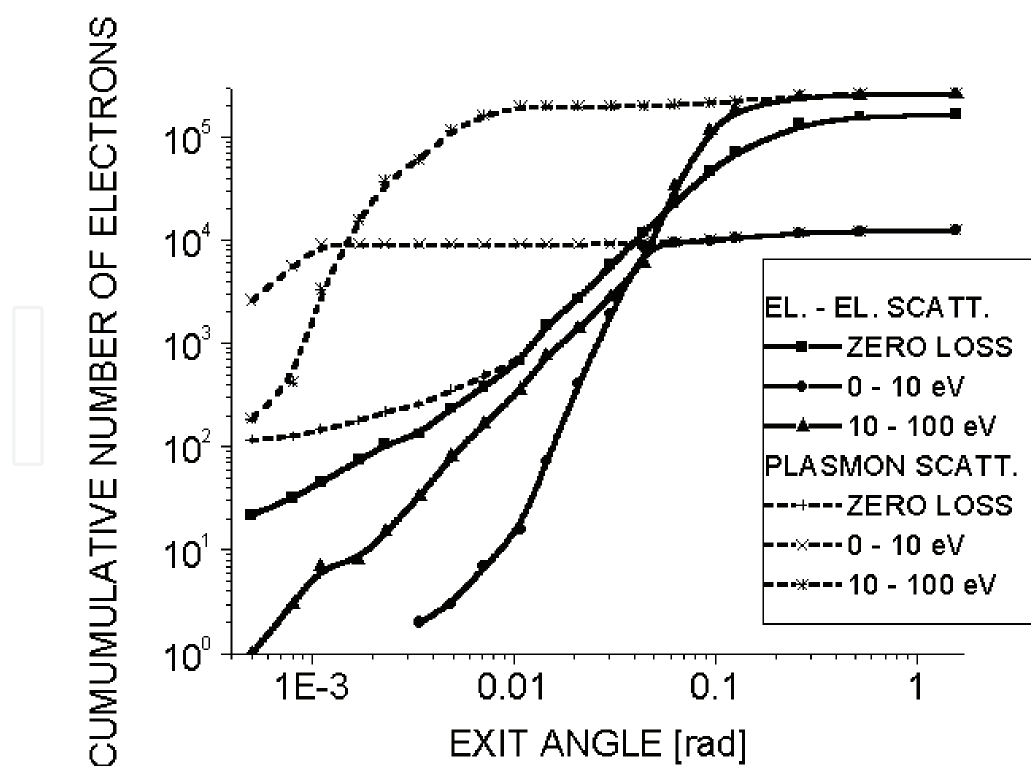

Fig. 12. Dependence of cumulative electron number of electrons transmitted through the film on objective aperture (thickness 10^{-6} g/cm^2).

3.6 Interaction volume

Among the most important parameters are the dimensions of the interaction volume, i.e., the dimensions of the volume at which the interaction of electrons with matter produces X-ray radiation. This quantity is important mainly when evaluating the composition of non-homogeneous samples, e.g., thin films on a substrate or particles in a matrix. Usually, the diameter of interaction volume D90 is defined as the diameter containing 90% of the produced (emitted) X-ray intensity. Simultaneously, the depth containing 90% of the produced (emitted) X-ray intensity can be defined as the information depth. Another definition of information depth and, simultaneously, a possible way of calculating it, is given by the decay of electron energy under the lowest energy necessary for excitation of a given X-ray radiation. This depth can be measured or estimated for example using the Bethe formula for stopping power. The actual diameter of the interaction volume can be experimentally measured by moving an electron beam across the sharp boundary of two materials of different composition and simultaneously detecting the signal from element contained only in one material. However, the interface sharpness must be guaranteed and interdiffusion must be avoided, which is not too simple. MC simulation can directly provide the distribution of X-ray production in matter (Murata et al., 1987) and (Kyser, 1989), and in this way can establish some limits of the dimensions of the interaction volume. The dimensions of the interaction volume should be compared with experimental estimations, but these values can be measured only indirectly and with relatively low precision; only the more or less precise semi-empirical formulas that are usually used provide only a rough estimation.

In our previous work (Starý, 2003) we have tried to define the dimensions of the interaction volume not only in homogeneous bulk samples, but also in case of film on the substrate. Moreover, we also tried to calculate their dependences on the electron energy and the thickness of the film. In this work, we used for calculation of the elastic DCS the PWADIR code with a muffin-tin model of atomic potential (Salvat & Mayol, 1993), the IMFP is obtained using optimization of the values of W_{min} (Starý, 2000), with W_{min} = 18.93 eV for Au and W_{min} = 9.52 eV for Si, so the obtained values of IMFP agree well with theoretical values given in (Tanuma et al., 1991a). Also the corrected Bethe stopping power was used. The surface plasmon excitation at input and output of the electron in the sample and also the energy losses at elastic collisions according to (Starý & Jurek, 2002) were taken into account. We simulated the process for a thin Au film on a thick Si substrate (i.e., not transmittable for electrons of the energies used). The electron beam energy was in the range 5 - 30 keV, the film thickness was in the range 0.05 - 1.0 μm. The number of primary electrons was relatively low (2000), but the number of inelastic collisions was 10^5 - 10^6. As the backscattering coefficient had a relative standard deviation of about 2%, we suppose the number of trajectories is reasonable for relatively reliable results. In the calculations, we copied the conditions of measurement, especially the take-off angle of the X-ray detector (TOA= 40°).

In the code, MC simulation of the electron trajectory in a stratified sample uses the algorithm for transmission of electrons into the next layer with different composition (Murata et al., 1987), with some corrections. In this model, the accumulated probability of collision increases during the electron path, and after transmission through the interface an electron can employ only the remnant of the accumulated probability; also, after transmission the electron keeps its direction. Also X-ray intensities were calculated in this work from the probability of photon emission at an inelastic collision. For characteristic

photon excitation, the Powell cross-sections (Powell, 1989) with the Schwaab coefficients (Schwaab, 1987) were used

$$\sigma_{c,P} = \sigma_o \frac{b_j Z_j}{E E_c} \ln\left(c_j \frac{E}{E_c} \right), \tag{37}$$

where E is the energy of an electron, E_c is the critical energy for ionisation of the shell in question, Z_j is the number of electrons in the j-th shell, and the constant $\sigma_o = 6.51 \times 10^{-20}$ keV^2 cm^2.

Because we have one element in the substrate and one element in the film, the actual element type is selected according to the position of electron (being either in film or in substrate). The ionisation probability is calculated at each inelastic scattering collision and at a given depth of the actual collision in sample z with actual electron energy. The intensity I_c of the element in question (i.e., the total number of photons of characteristic radiation of the element, detected in a solid angle $\Delta\Omega$ of a hypothetical detector, and generated by the given number of electrons) is then calculated as

$$I_c = \frac{1}{4\pi} N_1 \sigma_c \omega q t, \tag{38}$$

where $\sigma_c = \sigma_{c,P}$ is defined above, $N_1 = N_A\rho/A$, ω is the fluorescence yield calculated according to (Burhop, 1955), q is the ratio of the intensity of a measured line to the intensity of the whole X-ray line family (e.g., $I_{K\alpha}/(I_{K\alpha} + I_{K\beta})$, and t is the actual trajectory before collision. I_c is summed during the whole run of program. The intensity of the emitted radiation is calculated from the produced intensity, supposing the exponential decay of this intensity given by the mass absorption coefficients of the film and substrate (Goldstein, 1981) and taking into account the actual take-off angle of the detector.

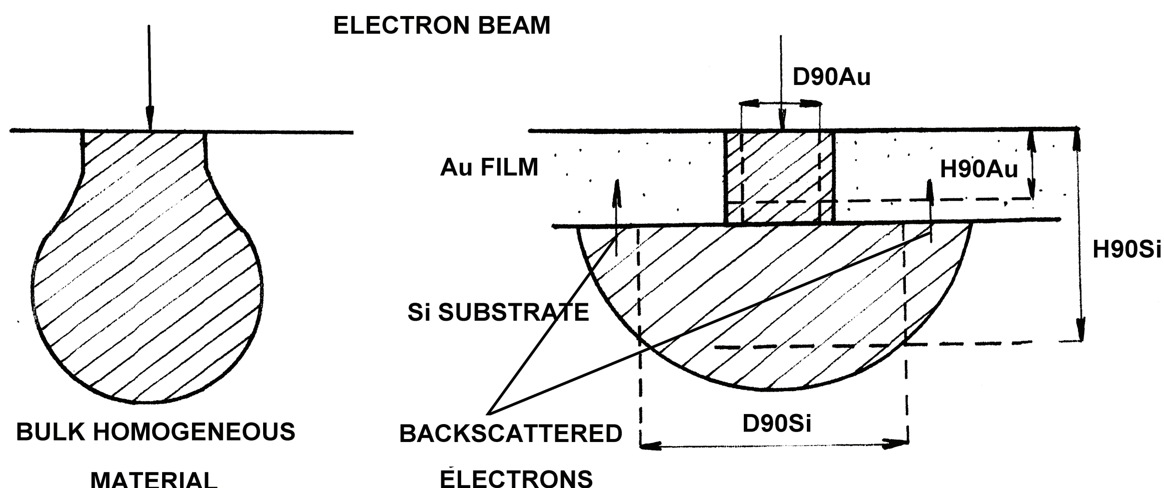

Fig. 13. The spectacular shape of the interaction volume, and definitions of the diameter of interaction volume D90 and the bottom depth of interaction volume H90.

We simulated the dependences of the dimensions of the interaction volume on the electron energy and film thickness. The volume distribution of the produced X-ray intensities gives the interaction volume in the sample. The spectacular shape of the interaction volume and

the definitions of the diameter of interaction volume D90 and the bottom depth of interaction volume H90 are shown in Figure 13. This Figure was drawn according to a qualitative image of the interaction volume, using the simple MC code from (Ly & Howitt, 1992). The interaction volume in the substrate in the vertical direction starts at the film/substrate interface and continues down into the substrate. In our code, the cell dimensions are defined in mass thickness units (g/cm^2) - in these units, the size for materials of different density is the same; the real size (e.g., in nanometers) is different.

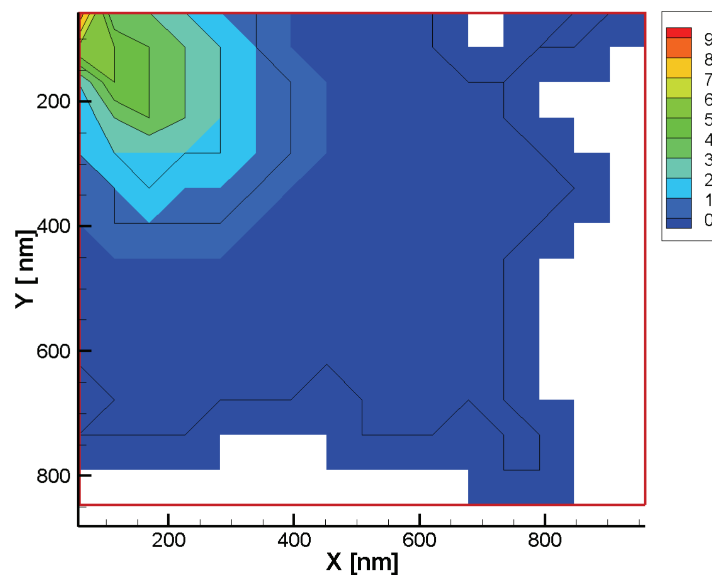

Fig. 14.a The interaction volume in bulk Au sample; E_0 = 20 keV. The intensities are integrated around the Y axis of image, electron beam of zero diameter hit the sample perpendiculary to the surface at left upper corner.

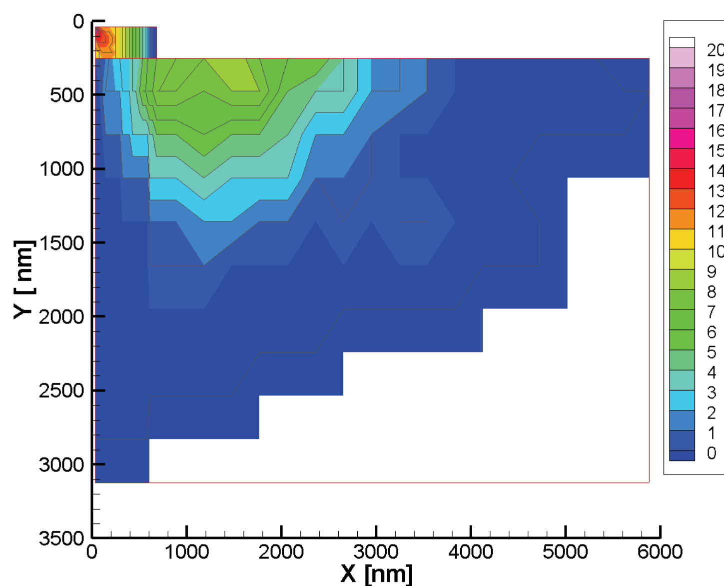

Fig. 14.b The interaction volume in the sample composed from thin film of Au on bulk Si sample; E_0 = 20 keV, film thickness ~ 250 nm. The same conditions of electron excitation, the different scale at the axis.

The Bethe range is the maximum supposed depth of electron interactions in the sample, and the maximum depth of X-ray production is limited by the energy necessary for X-ray excitation. Thus, firstly, the Bethe range and the maximum production depth in a layered structure composed of several elements are calculated. If the maximum production depth is lower than the whole sample thickness, its value is divided into 20 depth divisions. Otherwise, the sample thickness is divided in the same way. Next, radial division into 20 divisions of the same size is prepared. The X-ray produced radiation is placed into these cells, using the position of the actual inelastic collision; the intensities are calculated from the probabilities of X-ray radiation excitations. The intensities into radial cells are summed from the whole volume in a hollow cylinder of given dimensions, i.e., the signal is integrated over all azimuthal angles. The results for bulk Au target and for Si bulk sample with Au thin film are in Figures 14 a,b.

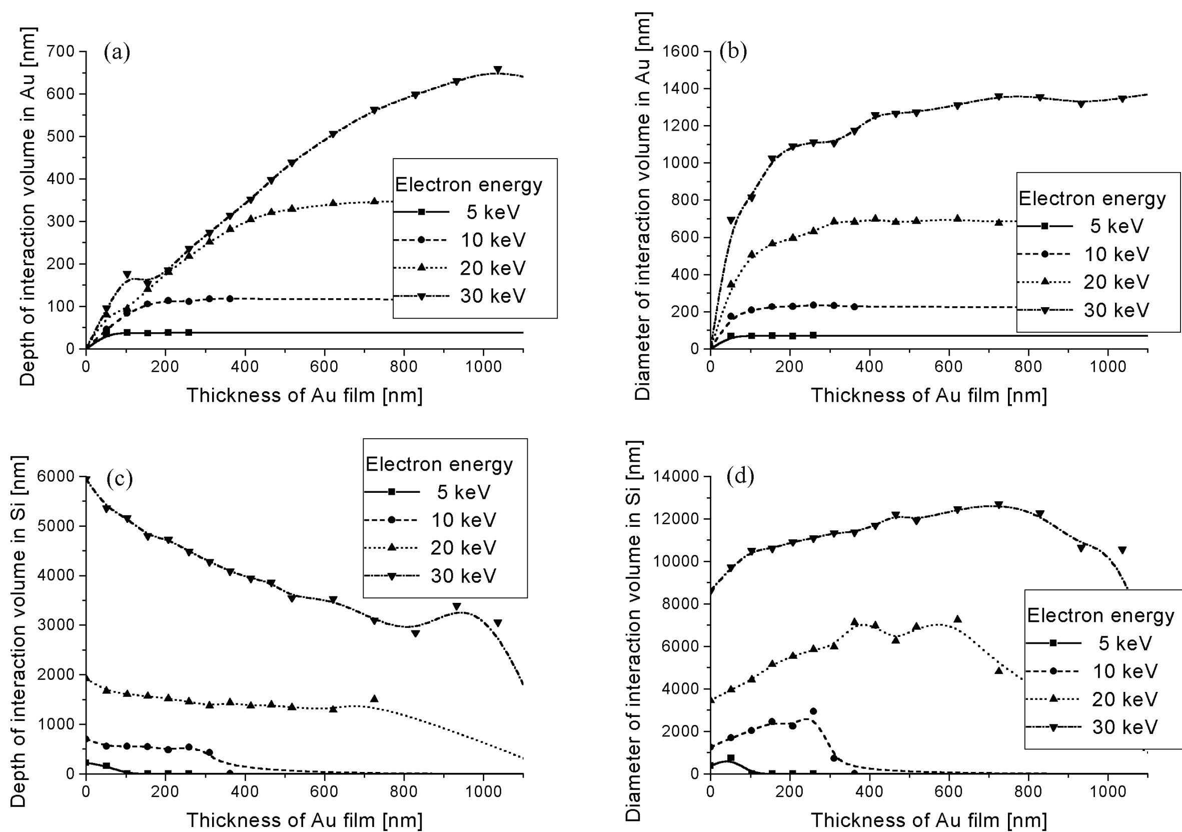

Fig. 15. Dependence of the depth and radius of the interaction volume on electron energy and film thickness: (a) depth of the interaction volume in the Au film (H90Au); (b) diameter of the interaction volume in the Au film (D90Au); (c) depth of the interaction volume in the Si film (H90Si); (d) diameter of the interaction volume in the Si film (D90Si).

Both radial and depth profiles of X-ray production in the samples were also calculated. Figure 15 shows the dependences of the depth and radius of the interaction volume on film thickness. Figure 15a shows that the depth of the interaction volume in the film material (H90Au) is limited by the film thickness, and increases with electron energy up to the value in pure Au (which is indicated at the thickness of Au film d_{Au} =1200 nm). The higher values of H90Au at the lowest thickness of Au film are given by the cell size value, because automatic division of interaction volume cannot position a cell exactly on the film/substrate

interface. The depth of the interaction volume in the Si substrate (H90Si) decreases from the value in pure Si due to the scattering in the Au film, which increases with Au film thickness. It is clear that at some thickness of the film no excitations proceed in the substrate; in this case H90Si reaches the zero value (though in the non-zero case the film thickness is added to H90Si - see the definition in Figure 13).

The diameter of the interaction volume in the Au film (D90Au) (Figure 15b) starts to increase relatively quickly with film thickness, and at a certain value of film thickness (depending on the electron energy) the rate of growth is suppressed and the D90Au remains constant (and approximately equal to the bulk Au value). The diameter of the interaction volume in substrate D90Si also increases with film thickness in the observed thickness range, due to the stronger elastic scattering of electrons in Au than the scattering in Si. The sudden fall to the final zero value appears at a thickness equal to the maximum depth of penetration of electrons at a given primary electron energy (see the case at electron energy 5 and 10 keV). At this thickness the Si X-ray produced intensity also falls to zero. The dimensions of the interaction volume in the substrate do not reflect in absolute scale the change in the excited X-ray intensity, which decreases substantially as the film thickness grows.

4. Discussion

Elastic peak electron spectroscopy (EPES) provides an opportunity both to study electron-matter interactions under special conditions of low and medium electron energy and also to define the material parameters near the surface. In most of works on this method, the relative EPES is utilized, where firstly the experimental values of elastic reflection coefficient is compared with Monte-Carlo calculated values for one element, at one electron energy and several supposed values of IMFP. The proper value of IMFP as then found by interpolation and IMFPs for other elements can be found by measurement of electron elastic reflection. By this way, a comparison of the obtained values of IMFP with theoretical values in general can give only a measure of the influence of the experimental conditions on the IMFP values.

We suggested a way to evaluate electron elastic reflection experiments, which is in principle similar to absolute EPES. The absolute EPES could give for any element the „experimental“ value of Bethe stopping power S_B and IMFP. Our method use experiment to find the optimal value of fitting parameter K using MC calculated and experimental $R_e(E)$ in some experimental energy range and calculation of $R_e(E)$ dependence by MC using these fitted values of K; the resulting value of K define the IMFP. Nevertheless, our calculations give the "integral" values of IMFP, where the *a priori* energy dependence of these quantities is supposed.

Conversely, the IMFP values obtained taking into account the surface energy losses (SEL) are substantially higher than both the NEL case and the theoretical values from TPP-2 (Fig. 6). In view of the presence of surface energy losses in the experiment, the relatively good agreement of theoretical and experimental+MC results without taking into account the surface energy losses seems not to be satisfactory. Formerly, it was assumed that in this case the resulting IMFP should be lower than the IMFP values obtained using the TPP-2 formula (Werner, 2001b). After switching to the next mechanism of energy losses, the elastic electron reflection decreases at the same IMFP. This is equivalent to the situation when, if we want to hold the experimental R_e values, IMFP must increase. From the theoretical presumptions in (Chen, 1996), (Vičánek, 1999), (Werner et al., 2003) it is known that the surface effect appears

near to the surface and the volume interactions are damped. This causes an increase of near surface IMFPs, given by volume interactions. The decrease in the volume interactions is partially compensated by the increase in the surface interactions. The provisional theory supposes that the increase in surface interactions compensates the decrease in volume interactions, thus the overall common effect is similar, as the volume interactions do not change at the surface; even though some surface interactions start after electrons have left the solid.

Our results can be explained by this model, if we adopt some more precise definitions of the obtained IMFPs. A simulation without taking the surface energy losses into account (NEL) shows the whole response of the solid, without separating the various sources of energy losses. According to theoretical suppositions, this response should be approximately equal to the bulk situation, which is proved by the good agreement of our values of IMFP, calculated using NEL condition, with TPP-2 values. In this way, we can take these values of IMFP as some „effective“ values in the vicinity of the surface. The calculated increased IMFPs, obtained under SEL conditions, show, in our opinion, the „real“ value of IMFP very near to the surface. Because in this case the surface interactions are taken into account separately, we suppose that the increase in IMFPs in comparison with TPP-2 can be explained by a real decrease in volume interactions near the surface, where most of the interactions proceed. Nevertheless, in this case the situation is rather complicated by the fact that the electron can move in various depths individually for each electron. The size of the interaction volume in which most of the scattering proceeds at low electron energy, can be obtained using MC calculation. Except of mean depth, the information depth, i.e., the depth from which 90% of elastically reflected electrons are coming from and the depth at which their last collision on an individual path took place, is calculated by our MC code. The mean depths of elastic collisions, the information depths and relative number of electrons, for which the deepest collision was in depth equal or less than 0.5 nm, for Al and Au and for several energies can be found. From this results we can see that 90% of the elastically reflected electrons come from the surface layer 3.04 and 4.2 nm in thickness (i.e., this is the information depth), respectively, for Al and 1.41 and 1.54 nm, respectively, for Au, for NEL and SEL, respectively, at 3 keV. Moreover, it is also shown that the relative number of backscattered electrons from the layer between the surface and a depth of 0.5 nm is relatively high both for Al and for Au, at least at low energy. As a consequence, the influence of surface vicinity on IMFP should decrease as the energy increases, when the depth of penetration increases. Our fitting method takes into account the whole energy region between 0.2 and 3 keV, without distinguishing this energy dependence.

There are several other possible reasons of differences between our values of IMFP and values from references. Due to the use of simple corrections of S_B, the differences of IMFP found by our method and the theoretical values from, mainly in the low energy region, could be caused by a difference between the corrected S_B and the theoretical values obtained using various more sophisticated stopping power calculations. If we compare the S_B values obtained by Bethe formula corrected for low energy with theoretical values, there are few differences between RSW and JL corrections of the Bethe stopping power for light elements (e.g., Al). In general, the JL corrected values of S_B are very near to the theoretical values given in (Ashley, 1988), (Ding & Shimizu, 1989) and (Fernandez-Varea et al., 1993). For Cu, our best fit gives the best agreement for values of S_B from (Fernandez-Varea et al., 1993). For heavier elements (e.g., Au), there are remarkable differences among various authors, and our stopping power calculated using the RSW correction (and giving the best agreement of

the MC result with experimental values of $R_e(E)$) agrees best with that calculated in (Fernandez-Varea et al., 1993). Nevertheless, the corrected S_B is in reasonable overall agreement with theoretical suppositions of stopping power for the observed materials.
Next, the experimental values of R_e at energies E > ~ 1 keV in (Schmid et al., 1983) are usually higher than the calculated values of R_e for all the elements. We suppose the reason could lie in the measurements using the RFA analyser. The relative resolution of the analyser used in this experiment increases with energy up to 5 eV at 2.5 keV (Schmid et al., 1983); in subsequent experiments (Dolinski et al, 1988a, 1988b and 1992), the resolution is estimated to be 0.6 %, i.e., 12 eV at 2 keV. Thus, some inelastically scattered electrons with low energy loss are treated as elastically scattered electrons. The surface plasmon of 3.4 eV is excited in Ag, which presence also could explain the large RMS for this element. In the calculation, all these electrons are excluded from the obtained value of R_e. By this way, the absolute EPES could give the "experimental" values of IMFP, but the measured values for usual measurements by RFA analysers are very strongly influenced by decreasing analyser resolution for higher energies.
The next disadvantage of EPES method for definition of IMFP is the influnce of IMFP value on possibility or intensity of surface excitations. As a consequence, the influence of surface vicinity on IMFP should decrease as the energy increases, when the depth of penetration increases. Our fitting method takes into account the whole energy region between 0.2 and 3 keV, without distinguishing this energy dependence.

5. Conclusion

In simulation of EPES experiment, we suggested a way to evaluate electron reflection experiments, which is in principle similar to absolute EPES. The particular results are as follows:

- In the model, there is only one fitting parameter K, which must be determined by comparison with measurement.
- Reasonably good agreement of calculated and experimental values of the elastic electron reflection coefficient was obtained in the energy region 0.2 - ~ 3 keV for the observed materials and suitable models.
- Selection of the best correction of the stopping power depends on the material.
- Incorporating surface energy excitations for MC calculations improves the agreement of R_e remarkably.
- The TFD model of elastic scattering is proved to be preferable for Al, Cu, Ag and Au.
- For IMFP, relatively good agreement with data in the literature was obtained without taking the surface excitations into account; in this case we obtained the "effective" IMFP near the surface, which defines the full response of a solid. Dividing the volume and surface excitations, we suppose that we obtained the real but "averaged" IMFP in the interaction volume near the surface, which is higher than the "effective" IMFP due to the decreasing influence of volume excitations. The depth dependence of this "averaged" IMFP cannot be determined at our way of evaluation.
- Using IMFP values from the literature for MC simulation of R_e dependencies, i.e., doing *ab initio* calculations, a comparison with experimental values indicates the medium or low influence of surface excitations, mainly for heavier materials. This proves that our method of IMFP's finding from experiment is relatively more efficient.

- Finally, the good agreement of the MC calculations with experimental values encourages the application of this fitting method to the study of IMFP and, generally, to the study of electron-matter interactions near the surface. For example, these calculations could be used to obtain the depth distribution of electron elastic collisions in solids.

Thus, our model of inelastic scattering might be reasonably appropriate for MC simulation of electron scattering by matter and for evaluation of IMFP from elastic electron reflection experiment at low electron energies.

Also the relatively good agreement in simulation of electron transmission through the thin films at the start of our work was obtained (the best using Hartree-Fockova atomic model for calculation of differential cross-sections of elastic scattering and simple hyperbolic model of electron inelastic scattering, without electron declination during scattering). Nevertheless, these simulations were realized at the start of our study, when better models were not available. In addition, with a low energy transmission electron microscope in a study of carbon, very good agreement with theoretical assumptions was found for the calculated angular distribution of elastically transmitted electrons in the given energy and thickness range. Using these results, the chromatic error was found, and in this way also the deterioration of resolution due to increasing sample thickness. Testing by measurement is necessary, but we believe the agreement of the experimental and calculated thickness and aperture dependences of transmitted electrons can be improved by implementing other models of energy losses into the code.

In our work on calculation of interaction volume, the MC data of electron backscattering and also of the k-ratios for thin films on substrate, in dependence on the energy of the electrons and on the film thickness, were compared with the experimental values, with reasonably good agreement. On the base of these findings, we have obtained reasonable estimations of the radial and vertical dimensions of the interaction volume and their dependence on the electron energy and on the film thickness. The results are important for Electron Probe Microanalysis of nonhomogeneous samples, e.g., for the analysis of films on substrates.

6. Acknowledgments

For a critical reading of this manuscript, for kind provission of experimental data and for helpful discussions, we would like to thank Dr. J. Zemek and Dr. J. Pavluch. This work was supported by Czech Science Foundation (GA-CR) projects No. 202/02/0237, No.101/06/0226, No. P108/10/1858 and project No. KAN101120701 of the Grant Agency of the Academy of Science of the Czech Republic. We are grateful to Mr Robin Healey for the large number of English language reviews.

7. References

Ashley J C. (1988). Interaction of low-energy electrons with condensed matter - stopping powers and inelastic mean free paths from optical-data. *J. Electr. Spectr. Rel. Phenom.*, Vol.46, (1988), 199, ISSN 0368-2048

Baró, J.; Sempau, J.; Fernandez-Varea, J.M.; Salvat F. (1995). PENELOPE - an algorithm for Monte-Carlo simulation of the penetration and energy-loss of electrons and positrons in matter. *Nucl. Instr. Meth.*, B Vol.100, (1995), p.31, ISSN: 0168-583X

Berger, M.J. (1963). In: *Methods Computational Physics*, Adler B., (Ed.), Vol. 1, 135, Acad. Press, ISBN 0124608019, New York

Berger, M.J.; Seltzer, J. (1964). Studies in penetration of charged particles in matter. Nucl. Sci. Ser. Rep. No. 39, NAS-NRC Publ. No. 1133, National Academy of Science, Washington DC, p. 205

Binder, K.(1979). Monte-Carlo Methods in Statistical Physics, Binder K., (Ed.), Springer, ISBN 0-387-16514-2, 3-540-16514-2, Berlin , (2. edition 1986).

Bote, D.; Salvat, F.; Jablonski, A.; Powell, C. J. (2009). The effect of inelastic absorption on the elastic scattering of electrons and positrons in amorphous solids. *Journal of electron spectroscopy and related phenomena*, Vol.175, (2009), pp.41-54, ISSN 0368-2048

Burhop B.H.S. (1955). *Journal de physique et le Radium*, Vol.16, (1955), p.625, ISBN ISSN 1160-8161

Cosslett, V.E.; Thomas, R.N. (1964a). Multiple scattering of 5-30 keV electrons in evaporated metals films. 1. Total transmission + angular distribution. *Br. J. Appl. Phys*., Vol.15, (1964), p.883, ISSN 0022-3727

Cosslett, V.E.; Thomas, R.N. (1964b). Multiple scattering of 5-30 keV electrons in evaporated metal films. 2. Range-energy relations. *Br. J. Appl. Phys*., Vol.15, (1964), p.1283, ISSN 0022-3727

Cosslett, V.E.; Thomas, R.N. (1965). Multiple scattering of 5-30 keV electrons in evaporated metal films. 3. Backscattering and absorption. *Br. J. Appl. Phys*., Vol.16, (1965), p.779, ISSN 0022-3727

Dapor, M. (2003). *Electron-Beam Interactions with Solids – Application of the Monte Carlo Method to Electron Scattering*, Springer, ISBN 3-540-00652-4, Berlin

Delong, A.; Kolarik, V.; Martin, D.C. (1998). Low voltage transmission electron microscope LVEM-5. *14th International Congress on Electron Microscopy, Electron Microscopy* 1998 Vol.1, pp.463-464, ISBN: 0-7503-0564-9, Cancun, Mexico, August 31-September 04, 1998

Ding, Z. J.; Shimizu, R. (1989). Inelastic-collisions of kV electrons in solids. *Surf. Sci.* Vol.222, (1989), p.313, ISSN 0039-6028

Dolinski, W.; Nowicki, H.; Mroz, S. (1988a). Application of elastic peak electron-spectroscopy (EPES) to determine inelastic mean free paths (IMFP) of electrons in copper and silver. *Surf. Interf. Anal.*, Vol.11, (1988), p.229, ISSN 0142-2421

Dolinski, W.; Mroz, S.; Zagorski, M. (1988b). Determination of the inelastic mean free-path of electrons in silver and opper by measurement and calculation of the elastic-scattering coefficient. *Surf. Sci.,* Vol.200, (1988), p.361, ISSN 0039-6028

Dolinski, W.; Mroz, S.; Palczynski, J.; Gruzza, B.; Bondot, P.; Porte, A. (1992). Determination of inelastic mean free-path of electrons in noble-metals. *Acta Phys Pol. A*, Vol.81, (1992), p.193, ISSN 0587-4246

Draper, N. R.; Smith H. (1966). *Applied Regression Analysis*, Willey, ISBN 0-471-22170-8, New York.

Fernandez-Varea, J.M.; Mayol R.; Liljequist, D.; Salvat F. (1993). Inelastic-scattering of electrons in solids from a generalized oscillator strength model using optical and photoelectric data. *J.Phys.: Condens. Matter*, Vol.5, (1993), 3593, ISSN 0953-8984

Fernandez-Varea, J.M.; Liljequist, D.; Csillag, S.; Räty, R.; Salvat, F. (1996). Monte Carlo simulation of 0.1-100 keV electron and positron transport in solids using optical data and partial wave methods. *Nucl. Instr. Meth.* B, Vol.108, (1996), p.35, ISSN 0168-583X

Fernandez-Varea, J.M.; Salvat, F.; Dingfelder, M.; Liljequist D. (2005). A relativistic optical-data model for inelastic scattering of electrons and positrons in condensed matter. *Nucl. Instr. Meth. B*, Vol.229, (2005), pp.187 –218, ISSN 0168-583X

Fitting, H-J. (1974). Transmission, energy-distribution, and se excitation of fast electrons in thin solid films. *Phys. Stat. Sol. A*, Vol.26 (1974) p.525, ISSN 0031-8965

Gauvin, R., l'Esperance, G. (1992). A Monte-Carlo code to simulate the effect of fast secondary electrons on k(ab) factors and spatial-resolution in the TEM. *Journal of microscopy-Oxford*, Vol.168, Part.2, (1992), p.153-167, ISSN 0022-2720

Goldstein J.I., Newbury D.E., Echlin P., Joy D.C., Fiori C., Lifshin E. (1981). *Scanning Electron Microscopy and X-Ray Microanalysis: a text for biologists, materials scientists, and geologists*, Plenum Press, ISBN 0-306-40768-X, New York, p. 620.

Chapman, J. N.; Gray, C. C.; Robertson B. W.; Nicholson W.A. P. (1983). X-ray-production in thin-films by electrons with energies between 40 and 100 keV. *X-ray Spectrometry,* Vol.12, (1983), p.153, ISSN 0049-8246

Chen, Y.F. (1995). Effect of surface excitations in determining the inelastic mean free-path by elastic peak electron-spectroscopy. *Journal of Vacuum Science & Technology A-Vacuum Surfaces and Films*, Vol.13, (1995), p.2665, ISSN 0734-2101

Chen, Y. F. (1996). Quantitative analysis in X-ray photoelectron spectroscopy: Influence of surface excitations. *Surf. Sci.,* Vol.345, (1996), p.213, ISSN 0039-6028

Chen, Y. F. (2002). Surface effects on angular distributions in X-ray photoelectron spectroscopy. *Surf. Sci.* Vol.519, (2002), p.115, ISSN 0039-6028

Inokuti, M. (1971). Inelastic collisions of fast charged particles with atoms and molecules - Bethe theory revisited. *Rev. Mod. Phys.,* Vol.43, (1971), p.297, ISSN 0034-6861

Jablonski, A., Salvat, F., Powell, C.J. (2003). NIST electron elastic-scattering cross-section database, version 3.1. NIST: Gaithersburg, MD

Joy, D. C.; Luo, S. (1989). An empirical stopping power relationship for low-energy electrons. *Scanning,* Vol.11, (1989), p.176, ISSN 0161-0457

Joy, D.C. (1995). *Monte Carlo Modeling for Electron Microscopy and Microanalysis*, Oxford University Press, ISBN 0-19-508874-3, Oxford

Jung, R.; Lee, J. C.; Orosz, G. T.; Sulyok, A.; Zsolt, G.; Menyhard, M. (2003). Determination of effective electron inelastic mean free paths in SiO2 and Si3N4 using a Si reference. *Surf. Sci.*, Vol.543, (2003), p.153, ISSN 0039-6028

Kirkpatrick, P.; Wiedmann, L. (1945). Theoretical continuous X-ray energy and polarization. *Phys. Rev.*, Vol.67, (1945), p.321, ISSN 0031-899X

Kissel, L.; Quarles, C. A.; Pratt. R. H. (1983). Shape functions for atomic-field bremsstrahlung from electrons of kinetic energy 1-500 keV on selected neutral atoms $1 \leq Z \leq 92$. *Atomic Data and Nuclear Data Tables,* Vol.28, (1983), p.381, ISSN 0092-640X

Kyser D.F. (1989) in: *Introduction to Analytical Electron Microscopy,* Hren J.J., Goldstein J.I., Joy D.C., (Eds.), p.199, Plenum Press, ISBN 0-306-40280-7, New York

Landau, L. D.; Lifshic, E. M. (1974). *Quantum Mechanics*, (translated from the Russian by J.B. Sykes and J.S. Bell). Pergamon Press, ISBN 0-08-017801-4, Oxford, p. 137

Lednicky, F.; Coufalova, E.; Hromadkova, J.; Delong, A.; Kolarik, V. (2000). Low-voltage TEM imaging of polymer blends. *Polymer*, Vol.41, (2000), p. 4909-4914, ISSN 0032-3861

Liljequist, D., (1978). Simplified models for monte-carlo simulation of energy-distributions of kev electrons transmitted or backscattered in various solids. *J. Phys. D: Appl. Phys.,* Vol.l1, (1978), p.839, ISSN 0022-3727

Liljequist D. (1983). A simple calculation of inelastic mean free-path and stopping power for 50 ev-50 kev electrons in solids. *J. Phys D: Appl. Phys.*, Vol.16, (1983), 1567, ISSN: 0022-3727

Ly, T.D.; Howitt, D.G. (1992). A Monte-Carlo calculation of the backscattering coefficient for a multilayer. *Scanning*, Vol.14, (1992), p.11, ISSN 0161-0457

Mayol, R.; Salvat, S. (1997). Total and transport cross sections for elastic scattering of electrons by atoms. *Atomic Data & Nuclear Data Tables,* Vol.65, (1997), p.55, ISSN 0092-640X

Murata, K.; Kawata, H.; Nagami K. (1987). Electron-scattering in low-voltage scanning electron-microscope targets. *Scanning Micr. Suppl.,* Vol.1, (1987), p.83, ISSN 0891-7035

Niedrig, H. (1982). Electron backscattering from thin-films. *J. Appl. Phys.*, Vol.53, (1982), p.R15, ISSN 0021-8979

Oswald, R. (1992). Numerische Untersuchung der elastischen Streuung von Elektronen an Atomen und ihre Rückstreuung an Oberflächen amorpher Substanzen im Energiebereich unter 2000 eV. PhD Thesis, Tuebingen. 173 p.

Penn, D.R. (1987). Electron mean-free-path calculations using a model dielectric function. *Phys.Rev. B* Vol.35. (1987). p.482, ISSN 0163-1829

Pines, D. (1964). *Elementary excitations in solids: lectures on phonons, electrons, and plasmons.* Benjamin, New York, ch. 3,4. ISBN

Powell, C.J. (1989). Cross-sections for inelastic electron scattering in solids. *Ultramicroscopy*, Vol.28, (1989), p.24, ISSN 0304-3991

Raether, H. (1980). *Excitation of Plasmons and Interband Transitions by Electrons.* Springer Tracts in Modern Physics 88 Spriger, ISBN 3-540-09677-9 - 0-387-09677-9, Berlin

Rao-Sahib, T. S.; Wittry, D. B. (1974). X-ray continuum from thick elemental targets for 10-50 keV electrons. *J. Appl. Phys.,* Vol.45, (1974), p.5060, ISSN 0021-8979

Reichelt, R.; Engel, A. (1984). Monte-Carlo calculations of elastic and inelastic electron-scattering in biological and plastic materials. *Ultramicroscopy*, Vol.13, (1984), p.279, ISSN 0304-3991

Reimer, L.; Brockmann, K., Rhein, U. (1978). Energy losses of 20 – 40 keV electrons in 150 – 650 $\mu g/cm^2$ metal films. *J. Phys D: Appl. Phys.*, Vol.11, (1978), p.165, ISSN:0022-3727

Reimer, L. (1984). *Transmission Electron Microscopy:* physics of image formation and microanalysis, Springer, ISBN 0-387-11794-6 , 3-540-11794-6, Berlin, p.138

Reimer, L.; Lodding, B. (1984). Calculation and tabulation of Mott cross-sections for large-angle electron-scattering. *Scanning,* Vol.6, (1984), p.128, ISSN 0161-0457

Reimer, L.; Stelter, D. (1986). Fortran-77 Monte-Carlo program for minicomputers using Mott cross-sections. *Scanning,* Vol.8, (1986) pp.265-277, ISSN 0161-0457

Reimer, L. (1996). Monte Carlo simulation techniques for quantitative X-ray microanalysis. *Microchimica Acta [Suppl.],* Vol.13, (1996), p.1, ISSN 0026-3672

Riley M.E. at al. (1975), *Atomic & Nuclear Data Tables*, Vol.15, (1975), p.443, ISSN 0092-640X

Ritchie, R.H. (1982). Energy-losses by swift charged-particles in the bulk and at the surface of condensed matter. *Nucl. Instr. and Meth.,* Vol.198, (1982), p.81, ISSN 0029-554X

Salvat, F.; Mayol, R. (1993). Elastic-scattering of electrons and positrons by atoms - Schrodinger and Dirac partial-wave analysis. *Comput. Phys. Commun.*, Vol.74, (1993), p.358, ISSN 0010-4655

Salvat, F.; Jablonski, A.; Powell, C. J. (2005). ELSEPA - Dirac partial-wave calculation of elastic scattering of electrons and positrons by atoms, positive ions and molecules. *Comput. Phys. Commun.,* Vol.165, (2005), p.157, ISSN 0142-2421

Shimizu, R.; Kataoka, Y.; Matsukawa, T.; Ikuta, T.; Murata, K.; Hashimoto, H. (1975). Energy-distribution measurement of transmitted electrons and Monte-Carlo simulation for kilovolt electron. *J. Phys. D: Appl. Phys.*, Vol.8, (1975), p.820, ISSN 0022-3727

Schmid, R.; Gaukler, H. K.; Seiler, H. (1983). Measurement of elastically reflected electrons (e-less-than-or-equal-to-2.5 kev) for imaging of surfaces in a simple ultra high-vacuum scanning electron-microscope. *Scan. Electr. Micr.*, Vol.2., (1983), 501, ISSN 0891-7035

Schwaab, P. (1987). Quantitative energy dispersive-x-ray microanalysis of thin metal specimens using the STEM. *Scanning*, Vol.9, (1987), p.1, ISSN 0161-0457

Starý, V. (1996). The check of the elastic scattering model in Monte-Carlo simulation. *Microscopica Acta A* Suppl.13, (1996), 559, ISSN 0026-3672

Starý, V. (1999). Fitting a Simple Model of Inelastic Scattering in Monte Carlo Code to Experimental Data. *J. Phys. D: Appl. Phys.,* Vol.32, (1999), pp.1811-1818, ISSN 0022-3727

Starý, V. (2000). Comparison of Monte Carlo simulation and measurement of electron reflection from solids. Proc. of MC2000 - Advanced Monte Carlo for Radiation Physics, Particle Transport Simulation and Applications, Kling A. et al. , (Eds.), p. 369, ISBN 3-540-41795-8, Lisbon, October 23-26, 2000

Starý, V.; Jurek, K. (2002). X-ray emission from thin films on a substrate - Calculation and experiments. *Microchimica Acta*, Vol.139, (2002), p.179, ISSN 0026-3672

Starý, V. (2003). Monte-Carlo Simulation of Electron Interaction with a Thin Film. *Thin Solid Films*, Vol.433, (2003), pp.326-331, ISSN 0040-6090

Starý, V.; Pavluch, J.; Zemek J. (2004). Monte-Carlo Simulation of Low-energy Electron Elastic Reflection by Solids – Assessment by Experiment, *42nd IUVSTA Workshop* '*Electron Scattering in Solids: From Fundamental Concepts to Practical Applications*', abstract in: S*urface and interface analysis*, Vol.38, (2006), p.88–117, Wiley InterScience, eISSN *1096-9918;* pISSN *0142-2421,* Debrecen, Hungary, July 4-8, 2004

Starý, V.; Zemek, J.; Pavluch J. (2007). Angular and energy distribution of backscattered electrons simulated by Monte-Carlo - Assessment by experiment I. *Vacuum*, Vol.82, (2007), pp.121-124, ISSN 0042-207X

Tanuma, S.; Powell, C. J.; Penn, D. R. (1987). Proposed formula for electron inelastic mean free paths based on calculations for 31 materials. *Surface Science*, Vol.192, (1987), p.L849-L857, ISSN 0039-6028

Tanuma, S.; Powell, C. J., Penn, D. R. (1991a). Calculations of electron inelastic mean free paths. 2. Data for 27 elements over the 50-2000 eV range. *Surface and Interface Analysis,* Vol.17, (1991), p.911, ISSN 0142-2421

Tanuma, S.; Powell, C. J., Penn, D. R. (1991b). Calculations of electron inelastic mean free paths. 3. Data for 15 inorganic-compounds over the 50-2000 eV range. *Surface and Interface Analysis,* Vol.17, (1991), p.927, ISSN 0142-2421

Tanuma, S.; Powell, C. J., Penn, D. R. (1993). Calculations of electron inelastic mean free paths. 4. Evaluation of calculated IMFPs and of the predictive IMFP formula TPP-2 for electron energies between 50 and 2000 eV. *Surface and Interface Analysis,* Vol.20, (1993), p.77, ISSN 0142-2421

Tanuma, S.; Powell, C. J., Penn, D. R. (1994). Calculations of electron inelastic mean free paths. 5. Data for 14 organic-compounds over the 50-2000 ev range. *Surface and Interface Analysis,* Vol.21, (1994), p.165, ISSN 0142-2421

Tougaard, S.(1997). Universality classes of inelastic electron scattering cross-sections. *J. Surf. Interface Anal.*, Vol.25, (1997), p.137, ISSN 0142-2421

Tung, C.J.; Ashley, J.C.; Ritchie, R.H. (1979). Electron inelastic mean free paths and energy-losses in solids. *Surf. Sci.*, Vol.81, (1979), p.427, ISSN 0039-6028

Vičánek, M. (1999). Electron transport processes in reflection electron energy loss spectroscopy (REELS) and X-ray photoelectron spectroscopy (XPS). *Surf. Sci.,* Vol.440, (1999), p.1, ISSN 0039-6028

Werner, W. S. M.; Smekal, W.; Tomastik, Ch.; Stori H. (2001a). Surface excitation probability of medium energy electrons in metals and semiconductors. *Surf. Sci.*, Vol.486, (2001), p.L461, ISSN 0039-6028

Werner, W. S. M. (2001b). Electron transport in solids for quantitative surface analysis. *Surface and Interface Analysis,* Vol.21, (2001), p.141, ISSN 0142-2421

Werner, W. S. M.; Eisenmenger-Sittner Ch.; Zemek J.; Jiricek P. (2003). Scattering angle dependence of the surface excitation probability in reflection electron energy loss spectra. *Phys. Rev. B,* Vol.67, (2003), p.155412, ISSN 1098-0121

IntechOpen

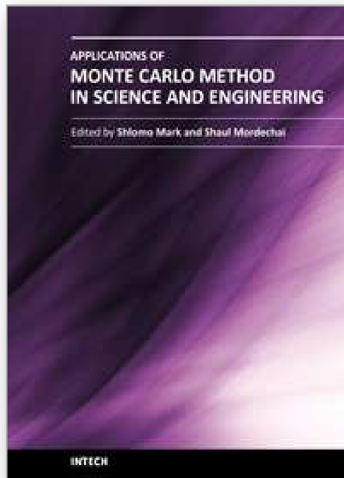

Applications of Monte Carlo Method in Science and Engineering

Edited by Prof. Shaul Mordechai

ISBN 978-953-307-691-1
Hard cover, 950 pages
Publisher InTech
Published online 28, February, 2011
Published in print edition February, 2011

In this book, Applications of Monte Carlo Method in Science and Engineering, we further expose the broad range of applications of Monte Carlo simulation in the fields of Quantum Physics, Statistical Physics, Reliability, Medical Physics, Polycrystalline Materials, Ising Model, Chemistry, Agriculture, Food Processing, X-ray Imaging, Electron Dynamics in Doped Semiconductors, Metallurgy, Remote Sensing and much more diverse topics. The book chapters included in this volume clearly reflect the current scientific importance of Monte Carlo techniques in various fields of research.

How to reference
In order to correctly reference this scholarly work, feel free to copy and paste the following:

Vladimîr Stary (2011). Monte-Carlo Simulation in Electron Microscopy and Spectroscopy, Applications of Monte Carlo Method in Science and Engineering, Prof. Shaul Mordechai (Ed.), ISBN: 978-953-307-691-1, InTech, Available from: http://www.intechopen.com/books/applications-of-monte-carlo-method-in-science-and-engineering/monte-carlo-simulation-in-electron-microscopy-and-spectroscopy

INTECH
open science | open minds

InTech Europe
University Campus STeP Ri
Slavka Krautzeka 83/A
51000 Rijeka, Croatia
Phone: +385 (51) 770 447
Fax: +385 (51) 686 166
www.intechopen.com

InTech China
Unit 405, Office Block, Hotel Equatorial Shanghai
No.65, Yan An Road (West), Shanghai, 200040, China
中国上海市延安西路65号上海国际贵都大饭店办公楼405单元
Phone: +86-21-62489820
Fax: +86-21-62489821

© 2011 The Author(s). Licensee IntechOpen. This chapter is distributed under the terms of the Creative Commons Attribution-NonCommercial-ShareAlike-3.0 License, which permits use, distribution and reproduction for non-commercial purposes, provided the original is properly cited and derivative works building on this content are distributed under the same license.

IntechOpen

IntechOpen